nature communications

Article

https://doi.org/10.1038/s41467-025-59972-z

CXCR4$^+$ mammary gland macrophageal niche promotes tumor initiating cell activity and immune suppression during tumorigenesis

Received: 14 March 2025

Accepted: 9 May 2025

Published online: 25 May 2025

Check for updates

Eunmi Lee[1,2], Jason J. Hong[1], Gabriel Samcam Vargas[1], Natalie Sauerwald[3,4], Yong Wei[1,2], Xiang Hang[1,2], Chandra L. Theesfeld[4], Jean Arly A. Volmar[4], Jennifer M. Miller[4], Wei Wang[4], Sha Wang[1], Gary Laevsky[1], Christina J. DeCoste[1] & Yibin Kang[1,2,5]

Tumor-initiating cells (TICs) share features and regulatory pathways with normal stem cells, yet how the stem cell niche contributes to tumorigenesis remains unclear. Here, we identify CXCR4$^+$ macrophages as a niche population enriched in normal mammary ducts, where they promote the regenerative activity of basal cells in response to luminal cell-derived CXCL12. CXCL12 triggers AKT-mediated stabilization of β-catenin, which induces Wnt ligands and pro-migratory genes, enabling intraductal macrophage infiltration and supporting regenerative activity of basal cells. Notably, these same CXCR4$^+$ niche macrophages regulate the tumor-initiating activity of various breast cancer subtypes by enhancing TIC survival and tumor-forming capacity, while promoting early immune evasion through regulatory T cell induction. Furthermore, a CXCR4$^+$ niche macrophage gene signature correlates with poor prognosis in human breast cancer. These findings highlight the pivotal role of the CXCL12-CXCR4 axis in orchestrating interactions between niche macrophages, mammary epithelial cells, and immune cells, thereby establishing a supportive niche for both normal tissue regeneration and mammary tumor initiation.

Tumor-initiating cells (TICs), often referred to as cancer stem cells (CSCs), share several key characteristics with normal stem cells, including self-renewal capacity and immune-privileged status[1–4]. It has long been speculated that regulators of normal stem cells may be exploited by TICs during the tumorigenesis and progression of many cancers, such as breast cancer, that originate from organs containing adult stem and progenitor cells[2,3,5].

The mammary gland is a highly dynamic organ that experiences numerous cycles of proliferation, differentiation, and apoptosis throughout a female's life[6,7]. The existence of mammary stem cells (MaSCs), which are capable of differentiating into three major mammary epithelial lineages, namely luminal secretory precursors, luminal hormone-sensing cells, and basal/myoepithelial cells, have long been speculated to play a key role in mammary gland

[1]Department of Molecular Biology, Princeton University, Princeton, NJ 08544, USA. [2]Ludwig Institute for Cancer Research Princeton Branch, Princeton, NJ 08544, USA. [3]Center for Computational Biology, Flatiron Institute, New York, NY 10010, USA. [4]Lewis-Sigler Institute for Integrative Genomics, Princeton University, Princeton, NJ 08544, USA. [5]Cancer Metabolism and Growth Program, Rutgers Cancer Institute of New Jersey, New Brunswick, NJ 08903, USA. e-mail: ykang@princeton.edu

development and homeostasis[8,9]. Earlier studies employing cleared fat pad transplantation assays and in vivo lineage tracing approaches have revealed the nature and hierarchy of postnatal MaSCs and progenitor cells under physiological conditions[6,10–13]. Several lines of evidence suggest that distinct populations of unipotent stem/progenitor cells are self-sustained and independently maintain the luminal and basal compartments of mammary glands[12–18], while other studies provided evidence for the presence of bipotent stem cells residing in the basal layers that can generate both luminal and basal lineages[8,9,19–24]. It is generally believed that while unipotent progenitor cells are primarily responsible for postnatal morphogenesis and homeostasis during adulthood, multipotent MaSCs are implicated in long-term ductal maintenance or tissue regeneration in response to injury[11]. Highly dynamic and heterogenous populations of MaSCs and progenitors may collectively contribute to mammary gland homeostasis.

Research in the past two decades, following the initial identification of MaSCs[8,9], has uncovered several MaSC-intrinsic regulators that also influence TIC activity and function during mammary tumorigenesis. These regulators include transcriptional factors such as SLUG[25], ELF5[26,27], and ΔNp63[28,29], miRNAs like miR-199a[30,31], cell surface receptors or ligands such as PROCR[22,32], and DLL1[23,33,34]. These factors govern self-renewal and differentiation signaling while also regulating local immune and stromal cell types to promote stemness and immune tolerance. However, little is known about the surrounding stromal components, or niches, that regulate MaSC and breast TIC activity.

Mammary gland macrophages have been previously shown to be essential for ductal morphogenesis during puberty, alveologenesis, pregnancy, and involution after weaning[35,36]. Our previous work identified mammary gland resident macrophages as crucial components of the MaSC niche[23]. Mechanistically, basal cells enriched with stem cell capacities exhibit a high expression level of the Notch ligand Delta-like 1 (DLL1), which activates the Notch signaling pathway in mammary gland macrophages. This activation induces the production of Wnt, feeding back to the MaSC-like basal cells to stimulate their stem/progenitor cell property[23]. Signals within the stem cell niche, including Notch and Wnt, typically involve short-range juxtacrine signaling[37,38]. This implies that macrophages and MaSCs must maintain close proximity and direct intercellular contact within the niche. Indeed, ductal macrophages were found to be intercalated between the luminal and myoepithelial layers and constantly monitor the epithelium through dendrite movement[39]. Furthermore, a recent study identified crosstalk between ductal macrophages and PROCR$^+$ MaSCs via IL1β-IL1R-NFkB signaling during estrus cycles and in response to cytotoxic stress, contributing to stem cell survival and activities[24]. However, key questions remain regarding which sub-population of mammary gland macrophages supports MaSC function, how these macrophages are recruited to the intraductal niche—typically separated from the surrounding stroma by the basement membrane (BM)[40,41]—and the mechanisms that initiate reciprocal niche signaling between niche macrophages and epithelial components to support mammary gland development.

Although the molecular links between MaSCs and breast TICs have been well established, the definition of TIC niches and how they contribute to mammary tumor initiation remains mostly unknown. The role of tissue-resident macrophages in tumor initiation remains controversial, largely due to the heterogeneous nature of macrophages across different tissues[42–46]. In this study, we elucidate the pivotal role of CXCL12–CXCR4 chemokine signaling in the intra-epithelial localization and the support of regenerative function of basal cells by mammary gland macrophages. CXCL12, derived from luminal epithelial cells, activates CXCR4 signaling in CXCR4$^+$ ductal macrophages, leading to AKT-mediated stabilization of β-catenin and its subsequent transcriptional activity. This signaling cascade results in increased MMP2, WNT2b, and Cyclin D, which facilitate the degradation of basement membranes and the migration of CXCR4$^+$ macrophages into the mammary epithelium, with enhanced ability to promote MaSC capacity of basal cells. Furthermore, we unveil the contribution of these macrophages to mammary tumor initiation and progression. Mammary gland CXCR4$^+$ macrophages are expanded during tumorigenesis and promote mammary tumor-initiating properties. Furthermore, they promote the formation of immunosuppressive niches through elevated expression of retinoid biogenesis enzyme ALDH1a2 and regulatory T cell (Tregs) induction. Generic depletion and pharmacological targeting of the CXCL12–CXCR4 axis inhibit tumor initiation, progression, and metastasis by reducing the number and activity of TICs, decreasing immune suppressive Tregs while increasing cytotoxic CD8 T cells. Our study reveals a chemokine-dependent interaction network essential for the recruitment and activation of ductal niche macrophages, thereby supporting MaSC/TIC functions during mammary gland development and mammary tumorigenesis.

Results

CXCR4-expressing mammary gland macrophages are adjacent to the mammary epithelium and are required for branching morphogenesis of the mammary gland

We previously showed that mammary gland macrophages have distinct molecular properties that support the self-renewal and proliferating potential of MaSCs while non-resident peritoneal macrophages are unable to do so[23]. This finding suggests that reciprocal interactions between mammary epithelial cells and macrophages are crucial for recruiting the latter into direct intercellular contact with the mammary epithelium. Additionally, these interactions provide specialized niche signals essential for the maintenance of MaSC functions throughout the development of the gland. We first compared the gene expression profiles[23] of mammary gland resident macrophages and peritoneal macrophages to identify candidate chemokine signaling molecules that could mediate such interactions. A list of genes encoding cytokines and chemokine receptors highly expressed in mammary gland macrophages was obtained, including CX3CR1 which was previously reported to be enriched in ductal macrophages of mammary glands[39]. Among these genes, *CXCR4* has the highest expression level based on RNAseq data and has the highest fold change in differential expression between mammary gland macrophages and peritoneal macrophages (Fig. 1a and Supplementary Table 1). Analysis of recently published single-cell RNA sequencing studies of mouse and human mammary gland[47,48] confirmed elevated expression of *CXCR4* in particular sub-populations (Ma in mice and m1 in humans) of mammary gland-resident macrophage (Supplementary Fig. 1a–f). In addition, we assessed the levels of *CXCR4* in ductal macrophages (DM) and stromal macrophages (SM), as identified in a recent study based on their respective physical locations[39] and found a higher *CXCR4* expression in duct-associated macrophages (Supplementary Fig. 1g); however, these previous studies did not investigate the importance of CXCR4 in the formation and function of the macrophageal niche for MaSCs.

Flow cytometry analysis verified the presence of CXCR4$^+$F4/80$^+$CD11b$^+$macrophages in mammary glands while CXCR4 expression is absent in non-resident peritoneal macrophages (Supplementary Fig. 2a). Subsequent analysis of CXCR4-expressing macrophages across various developmental stages of the mouse mammary gland indicated a notable increase in their numbers within the glands of 6-week-old mice (Fig. 1b). This elevated population level is sustained through the adult phase and undergoes additional increases during both pregnancy and the involution period (Fig. 1b). Immunofluorescence imaging of FFPE tissue sections from different developmental stages showed CXCR4-expressing macrophages localized near epithelial ducts (Fig. 1c and Supplementary. Fig. 2b). To assess the distribution of CXCR4-expressing macrophage in intact mammary gland tissue, we conducted three-dimensional (3D) confocal

https://doi.org/10.1038/s41467-025-59972-z

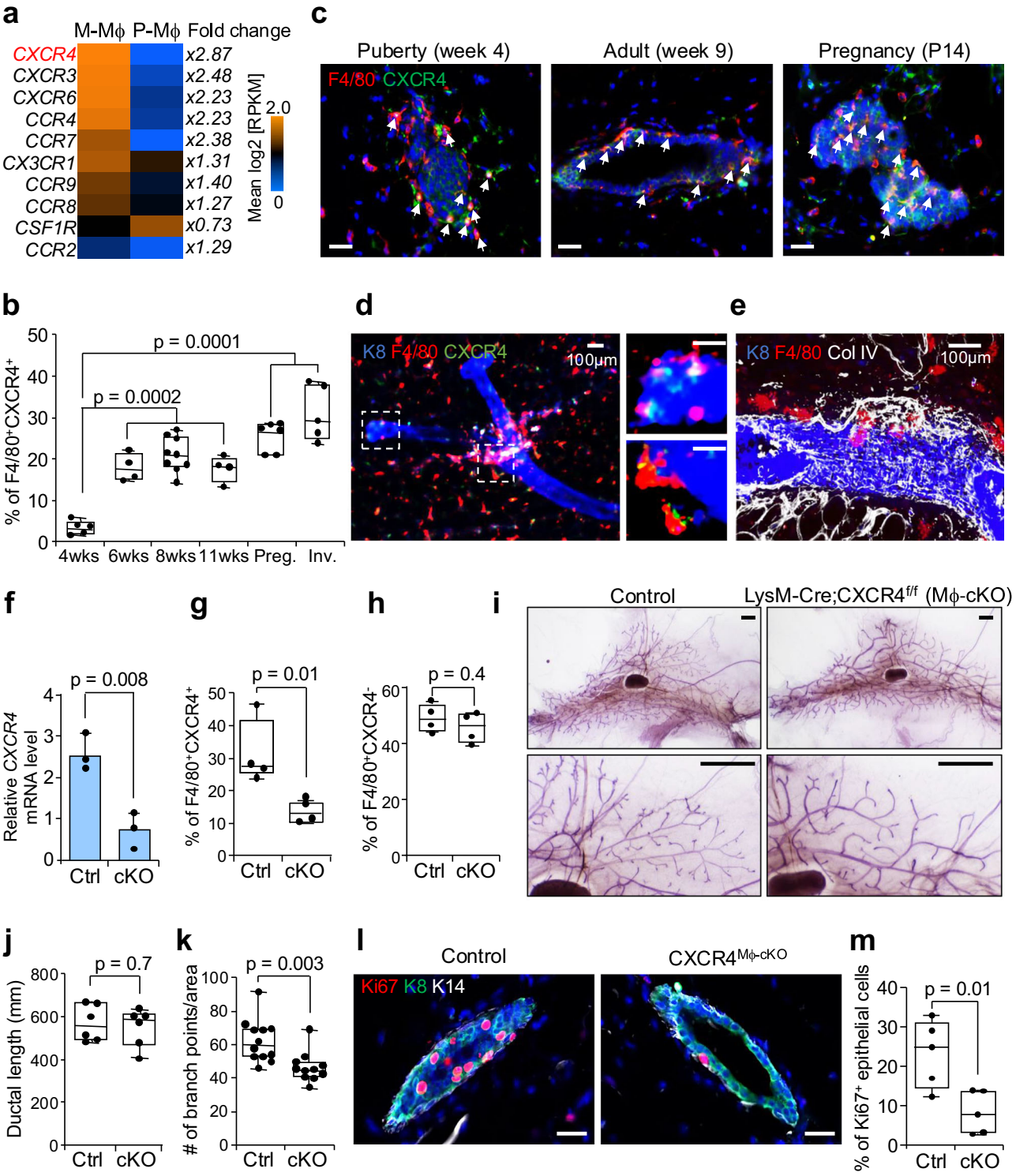

imaging of cleared mammary tissue after immunostaining of CXCR4 together with relevant lineage markers[39]. We again observed close proximity of CXCR4-expressing macrophages to epithelial ducts (Fig. 1d and Supplementary Fig. 2d), consistent with our previous report of mammary gland macrophages as a key component of MaSC niche[23] and a recent study showing intraductal localization of ductal macrophages[39]. Quantification of images confirmed the increased presence of CXCR4-expressing macrophages in the mammary ducts, and they are particularly enriched at the branching point and at the cleft of a dichotomous branching structure (Fig. 1d, Supplementary Fig. 2c, d, and Supplementary Movie 1). Co-immunofluorescent staining also confirmed penetration of F4/80$^+$ macrophages through the collagen IV- or Laminin-rich basement membrane to reach the mammary ductal epithelium (Fig. 1e, Supplementary Fig. 2e, f, and Supplementary Movie 2).

Next, we analyzed the expression of CXCR4 in a broader variety of cell types in the mammary gland and employed lineage-specific mouse genetic knockout models to evaluate the functional significance of CXCR4 expression in macrophages for mammary gland development. While qRT-PCR data and single-cell RNA sequencing (scRNA-seq) analysis of normal mouse mammary gland, as well as scRNA-seq analysis of human breast tissue[47], revealed high *CXCR4* gene expression in

Fig. 1 | Genetic depletion of CXCR4 in mammary gland macrophage inhibits mammary branching morphogenesis. a Heatmap showing differentially expressed chemokine/cytokine receptor genes between mammary gland macrophages (M-Mϕ) and peritoneal macrophages (P-Mϕ), with fold changes indicated. **b** Percentage of F4/80$^+$CXCR4$^+$ Mϕ among CD11b$^+$ cells (Supplementary Fig. 16b) in mammary glands from different stages (n = 4, 5, 6, 9, biologically independent samples, Wks weeks, Preg. pregnancy, Inv. involution). **c** Immunofluorescence (IF) images of mammary gland at puberty (week 4), adult (week 9), and pregnancy (P14), stained for CXCR4 (green) and F4/80 (red). White arrows indicate double-positive cells. **d**, **e** Whole-mount mammary gland tissues from 8-week-old females stained for **d** Keratin 8 (K8, blue), F4/80 (red), and CXCR4 (green) or **e** Keratin 8 (K8, blue), F4/80 (red), and Collagen IV; Col IV (white). Enlarged views of boxed areas are shown. **f** qRT-PCR analysis of *CXCR4* mRNA expression in Mϕ from LysM-Cre littermate control (Ctrl) and CXCR4$^{Mϕ\text{-}cKO}$ mice (cKO) (n = 3, biologically independent samples). **g**, **h** Flow cytometry quantification of F4/80$^+$CXCR4$^+$ Mϕ among CD11b$^+$ cells (**g**) and F4/80$^+$CXCR4$^-$ Mϕ among CD11b$^+$ cells (**h**) (Supplementary Fig. 16b) in LysM-Cre littermate control and CXCR4$^{Mϕ\text{-}cKO}$ mice. F4/80$^-$CXCR4$^-$ and F4/80$^-$CXCR4$^+$ cells among CD11b$^+$ cells are excluded from the quantification graph (n = 4, biologically independent samples). **i** Representative images of carmine alum whole mount staining of mammary glands from control and CXCR4$^{Mϕ\text{-}cKO}$ mice (8 weeks). **j**, **k** Quantification of **j** ductal length (n = 6, biologically independent samples), **k** branching (n = 11, 12, biologically independent samples). **l** Ki67, K8 and K14 staining of control and CXCR4$^{Mϕ\text{-}cKO}$ mammary glands. **m** Quantification of Ki67+ cell percentage among total epithelial cells in the field of view (n = 6, biologically independent samples). Scale bar, 50 μm in (**c**, **l**), 100 μm in (**d**, **e**), and 25 μm in (**i**). Data are mean values ± s.d. Statistical significance was calculated by two-tailed unpaired Student's t-test or one-way ANOVA with Turkey's test. Box plots show the median (center line), 25th/75th percentiles (box bounds), whiskers extending to 1.5× IQR, and outliers plotted individually. Source data are provided as a Source Data file.

mammary gland macrophages, other immune cells such as T cells, B cells, and NK cells also expressed CXCR4. Notably, mammary epithelial cells and other non-immune stromal cells such as fibroblasts express little or much lower levels of CXCR4 (Supplementary Fig. 3). To rule out the potential impact of other CXCR4-expressing non-macrophage cells on mammary gland development, we generated myeloid cell-specific, LysM-Cre mediated CXCR4 conditional knockout mice (CXCR4$^{Mϕ\text{-}cKO}$) by crossing LysM-Cre transgenic mice[49] with CXCR4 floxed mice[50]. Significantly reduced CXCR4 expression in the mammary gland macrophages of knockout mice and reduced percentage of CXCR4$^+$ macrophage was confirmed by qRT-PCR and flow cytometry assay, respectively (Fig. 1f–h, and Supplementary Fig. 4a). LysM-Cre-mediated CXCR4 deletion did not affect the number of other immune populations, including neutrophils, monocytes, or lymphoid CD8$^+$ T, CD4$^+$ T, NK and B cells (Supplementary Fig. 4b and c). We observed that most non-macrophage immune cells and lineage-negative mammary epithelial cells in mammary glands exhibited very low or no CXCR4 expression, except for B cells (Supplementary Fig. 4d–f). In addition, CXCR4 levels remained unchanged in CXCR4-expressing non-macrophage cell types such as B cells, luminal and basal epithelial cells in the mammary gland of CXCR4$^{Mϕ\text{-}cKO}$ mice (Supplementary Fig. 4g–i). Furthermore, CXCR4 deletion by LysM-Cre does not impact other tissue-resident macrophages, including those in the liver, lungs, and spleen. The overall weight of these tissues as well as the percentage of total macrophages showed no significant differences. Lung and spleen-resident macrophages exhibited little to no CXCR4 expression, while liver macrophages expressed CXCR4 at much lower levels compared to mammary gland macrophages (Supplementary Fig. 4j–l). Collectively, these results demonstrate macrophage-specific depletion of CXCR4 in the knockout mice and the lack of impact on other cell types. Notably, we observed a significant reduction in ductal branching formation and the number of terminal end buds in CXCR4$^{Mϕ\text{-}cKO}$ mice compared to littermate controls, whereas mammary ductal elongation was not significantly affected (Fig. 1i–k, Supplementary Fig. 4m and n). Immuno-staining of Ki67 revealed fewer proliferating epithelial cells in the mammary glands of CXCR4$^{Mϕ\text{-}cKO}$ mice (Fig. 1l, m). These results indicate that CXCR4 expression in mammary duct-associated macrophages plays important roles in branching morphogenesis and proliferation of mammary epithelium.

Loss of CXCR4 in macrophages prevents their migration into intraductal spaces

Next, we evaluated the number, localization, and function of the mammary gland macrophages in littermate controls and CXCR4$^{Mϕ\text{-}cKO}$ mice. The number of F4/80$^+$CD11b$^+$ macrophages as measured by flow cytometry analysis was not significantly changed after CXCR4 knockout in macrophages (Fig. 2a). Immunostaining of mammary gland sections demonstrated that F4/80$^+$ macrophages are commonly situated near the mammary ducts and exhibit a close association with the mammary epithelial layer (Fig. 2b, left panel). In contrast, while F4/80$^+$ macrophages were detected near the ducts in the mammary glands of CXCR4$^{Mϕ\text{-}cKO}$ mice, they predominantly remained outside the epithelial layer (Fig. 2b, right panel). Quantification of intra-epithelial localization of macrophages confirmed significantly reduced interactions between macrophages and epithelial cells in CXCR4$^{Mϕ\text{-}cKO}$ mice (Fig. 2c). Notably, we also observed macrophages with an elongated morphology exclusively within control mammary glands, particularly when in close association with epithelial cells. This elongated macrophage phenotype has been previously identified as a response to a variety of local environmental signals. It facilitates the formation of an intercellular network and plays a crucial role in mediating numerous molecular signaling processes, including macrophage polarization[51,52].

Given the reduced presence of CXCR4$^{Mϕ\text{-}cKO}$ macrophages in the intraepithelial space, we first assessed the migratory property of macrophages with or without genetic knockout of CXCR4. Transwell migration assay using macrophages isolated from mammary glands of control and CXCR4$^{Mϕ\text{-}cKO}$ mice showed reduced migration of CXCR4$^{Mϕ\text{-}cKO}$ mammary gland macrophages compared to control cells in vitro (Fig. 2d and Supplementary Fig. 5a). To characterize the molecular features of control and CXCR4$^{Mϕ\text{-}cKO}$ macrophages, we isolated them from adult mouse mammary glands by fluorescence activating cell sorting (FACS) and performed RNA sequencing analysis. Gene set enrichment analysis (GSEA) of transcriptomic data showed that, compared to CXCR4-deficient macrophages, control macrophages are enriched for cell migration-related gene signatures (Supplementary Fig. 5b), with elevated expression of genes known to promote macrophage motility and adhesion in both physiological and pathological settings (Fig. 2e). CXCR4 loss, however, did not affect the expression of CCL2/CCR2 and CSF1/CSF1R, major known regulators of macrophage trafficking.

As both CXCR4$^-$ and CXCR4$^+$ macrophages exist in the wild-type mammary gland (Supplementary Fig. 2a), we directly evaluated the migration ability of these populations by transwell migration assay with FACS-isolated CXCR4$^-$ and CXCR4$^+$ mammary gland macrophages. Indeed, CXCR4$^+$ macrophages showed higher migration capacity than CXCR4$^-$ macrophages in vitro (Fig. 2f). Similar RNAseq gene expression profiling was performed on CXCR4$^+$ and CXCR4$^-$ macrophages. Gene ontology pathway analysis showed that CXCR4-expressing macrophages are enriched for migration and chemotaxis-related pathways (Fig. 2g). Furthermore, distinct signaling pathways involved in immune regulation and metabolism were shown between two cells, suggesting that CXCR4 expression marks a specific macrophage sub-population that has distinct molecular features (Supplementary Fig. 5c and d).

CXCR4 depletion in macrophages suppresses the function of mammary gland stem cells

The impaired branching formation and reduced ductal epithelial cell proliferation shown in CXCR4$^{Mϕ\text{-}cKO}$ suggested that CXCR4 depletion in

https://doi.org/10.1038/s41467-025-59972-z

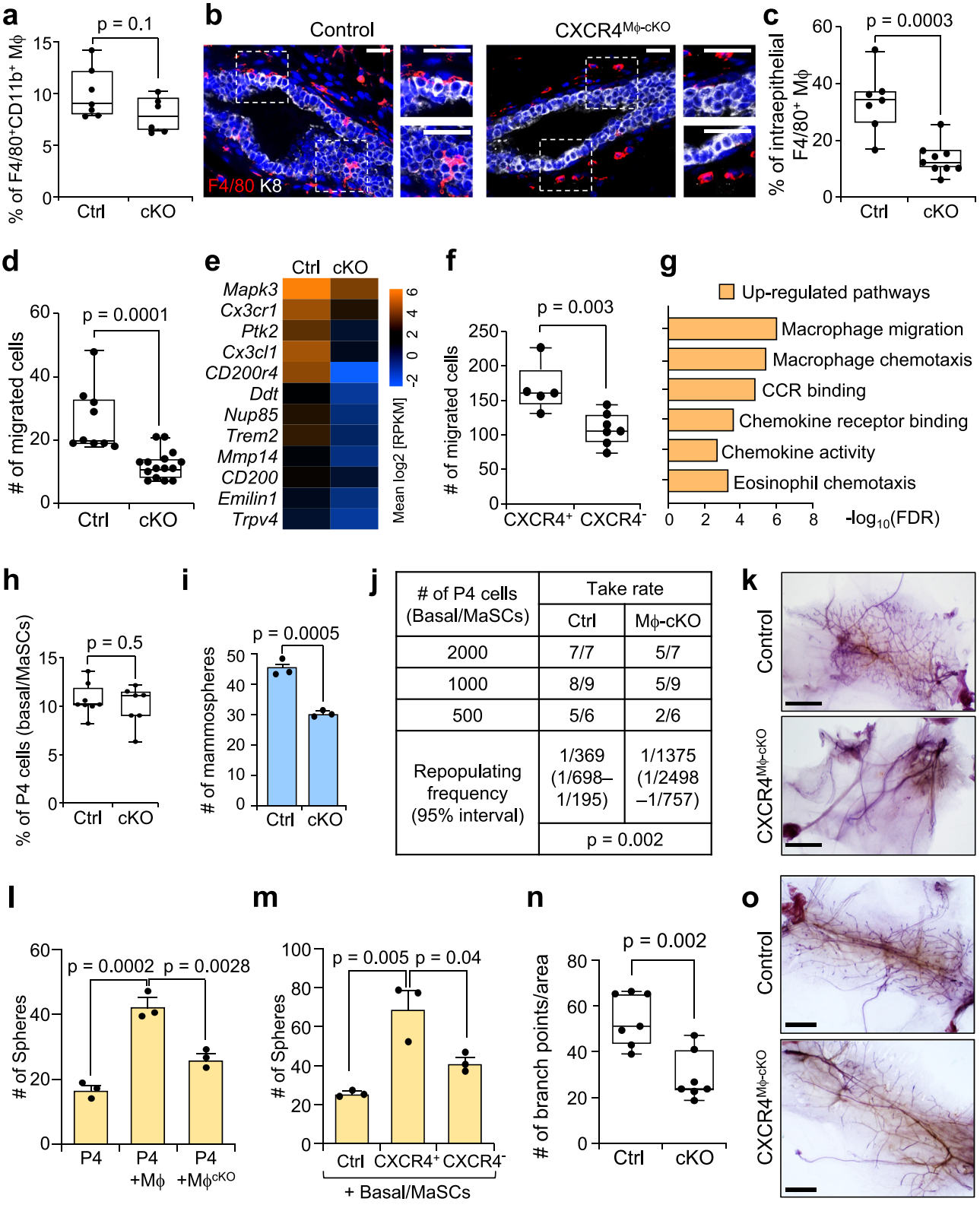

macrophages might suppress the MaSC function. Building on our previous study showing a critical interaction of MaSCs and macrophages via juxtracrine Notch and Wnt signaling for the maintenance of MaSC survival and functionality during mammary gland developments[23], we proceeded to examine the number and growth of MaSCs in the mammary gland of CXCR4$^{Mϕ\text{-}cKO}$ mice using a set of established assays as previous reported[8,26,28]. Lin$^-$CD24$^+$CD29^{high} (P4) MaSC-enriched basal population was analyzed by flow cytometry and sorted for assessing regenerative growth capacity using in vitro mammosphere formation assay in ultralow-attachment plates and limited dilution cleared fat pad repopulation assay in vivo (Supplementary Fig. 6a). Although we detected no difference in the number of Lin$^-$CD24$^+$CD29^{high} (P4) MaSC-enriched basal population (Fig. 2h and Supplementary Fig. 6b), FACS-isolated P4 populations from mammary glands of CXCR4$^{Mϕ\text{-}cKO}$ mice formed significantly fewer mammospheres in vitro, compared to cells from control mice (Fig. 2i), indicating

Fig. 2 | CXCR4 is critical for macrophage-mediated stem cell promoting activity. a F4/80$^+$ Mϕ among CD11b$^+$ cells (Supplementary Fig. 16c) in control and CXCR4$^{Mϕ\text{-}cKO}$ mammary glands ($n = 6, 7$, biologically independent samples). **b** F4/80 and K8 IF staining of control and CXCR4$^{Mϕ\text{-}cKO}$ mammary glands. Enlarged views of boxed areas are shown. **c** Quantification of intraepithelial F4/80$^+$ cells per field ($n = 4$, biologically independent samples, 3 ductal areas were randomly selected per each section). **d** Transwell migration assays of control and CXCR4$^{Mϕ\text{-}cKO}$ macrophages ($n = 4$, biologically independent samples, 5 microscopic fields were randomly selected from each well). **e** Heatmap of differentially expressed genes (DEGs) related to macrophage migration from RNA-seq of control and CXCR4$^{Mϕ\text{-}cKO}$ Mϕ. **f** Transwell migration of CXCR4$^+$ and CXCR4$^-$ macrophages ($n = 3$, biologically independent samples, 5 microscopic fields were randomly selected). **g** Pathway enrichment analysis from DEGs in CXCR4$^+$ vs. CXCR4$^-$ macrophages, highlighting migration/Chemotaxis pathways ranked by adjusted FDR. **h** Quantification of Lin$^-$CD24$^+$CD29^{Hi} Basal/MaSCs (P4) cells (Supplementary Fig. 16a) from control and CXCR4$^{Mϕ\text{-}cKO}$ mammary glands ($n = 7$, biologically independent samples). **i** Mammosphere formation of 5000 P4 cells from control and CXCR4$^{Mϕ\text{-}cKO}$ mice ($n = 3$, biologically independent samples). **j** Limited dilution assay with P4 cells from control and CXCR4$^{Mϕ\text{-}cKO}$ mammary glands. Table representing serial dilution injections with the corresponding take rate and repopulation frequencies (calculated by ELDA, Pearson's Chi-squared test, two-sided). **k** Representative Carmine alum-stained mammary outgrowths. **l**, **m** Mammosphere formation assay using 5000 P4 cells cocultured with **l** 20,000 Mϕ from control and CXCR4$^{Mϕ\text{-}cKO}$, or **m** 20,000 CXCR4$^+$ and CXCR4$^-$ Mϕ ($n = 3$, biologically independent). **n** Limited dilution assay of WT P4 injected into control and CXCR4$^{Mϕ\text{-}cKO}$ recipient mice; ductal branching quantified ($n = 7$, biologically independent samples). **o** Representative mammary outgrowths. Scale bar, 50 μm in (**b**) and 25 μm in (**k**) and (**o**). Data are mean values ± s.d. Statistical significance was calculated by two-tailed unpaired Student's *t*-test or one-way ANOVA with Turkey's test. Box plots show the median (center line), 25th/75th percentiles (box bounds), whiskers extending to 1.5× IQR, and outliers plotted individually. Source data are provided as a Source Data file.

reduced stem/progenitor activity. We further performed limiting dilution cleared fat pad reconstitution assay to directly test the regeneration potential of the MaSC-enriched P4 populations in vivo. The results showed that CXCR4$^{Mϕ\text{-}cKO}$ mice-derived P4 cells had a significantly decreased repopulating ability, confirming the reduced MaSC function of these cells in CXCR4$^{Mϕ\text{-}cKO}$ mice (Fig. 2j, k). Consistent with these phenotypic differences, several stem cell transcription factors and markers, such as *Dll1*[23], *ΔNp63*[28], *Sox9*[25], and *Bcl11b*[53] showed consistently reduced expression in P4 cells from CXCR4$^{Mϕ\text{-}cKO}$ mammary epithelium compared to those from the littermate control (Supplementary Fig. 6c).

We next considered that CXCR4 deficiency may alter cellular and molecular properties of the resident macrophages, which could lead to impaired MaSC functions as observed above. We previously developed an in vitro mammosphere co-culture assay in which mammary gland macrophages promote sphere formation of MaSCs[23]. To test the effect of CXCR4 depletion on the ability of macrophages to promote stem cell growth, we co-cultured Lin$^-$CD24$^+$CD29^{high} MaSC-enriched basal cells with mammary gland macrophages from controls and CXCR4$^{Mϕ\text{-}cKO}$ mice and measured sphere formation (Supplementary Fig. 6a). Macrophages from CXCR4$^{Mϕ\text{-}cKO}$ mice demonstrated reduced efficacy in facilitating mammosphere formation by MaSC-enriched basal cells when compared to control macrophages (Fig. 2l). GSEA revealed a decreased enrichment of gene signatures related to Notch signaling as well as mammary gland-associated macrophage signature on macrophages derived from CXCR4$^{Mϕ\text{-}cKO}$ mice (Supplementary Fig. 6d). Consistently, the expression of key Notch/Wnt signaling genes, such as *Wnt2b*, *Wnt6* and *Jag2* were reduced in macrophages lacking CXCR4 (Supplementary Fig. 6e). These results indicate that a down-regulation of Notch/Wnt signaling activity in macrophages from CXCR4$^{Mϕ\text{-}CKO}$ mice adversely affected its stemness-promoting function.

We also co-cultured Lin$^-$CD24$^+$CD29^{high} MaSC-enriched basal cells with CXCR4$^+$ or CXCR4$^-$ macrophages to compare the MaSC-promoting activity of mammary gland macrophages with different status of CXCR4 expression. Although both types of macrophages were capable of promoting mammosphere formation by MaSCs, the CXCR4-positive macrophages exhibited significantly greater efficacy in stimulating this process (Fig. 2m).

To further validate the influence of CXCR4-expressing macrophages in the mammary gland stem cell niche, we conducted a cleared fat pad reconstitution assay by injecting wild-type MaSC/basal cells into controls and CXCR4$^{Mϕ\text{-}cKO}$ mice. Wild-type MaSCs could repopulate the mammary glands in both recipients. However, we observed a significantly diminished number of branches in the reconstituted mammary glands of CXCR4$^{Mϕ\text{-}cKO}$ recipients, suggesting that CXCR4-deficient macrophageal niche could not sufficiently support MaSC-mediating branching morphogenesis (Fig. 2n, o). Altogether, these results indicate that the loss of CXCR4 leads to a failure in positioning macrophages close to the stem cell niche, as well as a disruption of the Notch/Wnt-dependent signaling required for sustaining MaSC capacity during mammary branching morphogenesis.

Chemokine CXCL12 produced by luminal epithelial cells is pivotal to mammary gland ductal morphogenesis

The CXCR4 chemokine receptor is activated by the cognate chemokine CXCL12 to initiate downstream signals, such as migration and proliferation[54,55]. We next sought to determine the cellular source of CXCL12 that attracts CXCR4$^+$ macrophages to the mammary epithelium. To this end, we first analyzed the expression of CXCL12 in mammary gland epithelial cells. Our previous gene expression analysis of mammary gland epithelial cells[23,30] revealed that the level of *CXCL12* is 13-fold greater in MaSC-enriched basal cells, compared to luminal cells (Supplementary Fig. 7a). qRT-PCR assay validated the higher *CXCL12* mRNA in MaSC/basal cells (Supplementary Fig. 7b). Next, we measured CXCL12 protein expression and its localization in the mammary epithelium. Surprisingly, immunofluorescent staining of CXCL12 together with either basal marker, Keratin-14 (K14), or luminal marker, Keratin-8 (K8) revealed co-localization of CXCL12 with K8-expressing luminal cells, instead of K14-positive basal cells (Fig. 3a). To validate this discordant mRNA and protein expression of CXCL12 in basal and luminal cells, we took advantage of a technique, PrimeFlow, to simultaneously detect mRNA and protein levels in single cells by flow cytometry analysis. Consistently, luminal cells showed a higher protein expression of CXCL12 protein whereas MaSC/basal cells with a higher *CXCL12* mRNA exhibited a lower protein level (Fig. 3b). We further confirmed the expression of CXCL12 in estrogen receptor (ER) and progesterone receptor (PR)-positive luminal cells (Supplementary Fig. 7c). This is consistent with the previous finding that CXCL12 is highly localized with PR$^+$ luminal cells[56]. Immunostaining of mammary glands from different stages—normal, pregnancy, lactation, and involution—indicated that CXCL12 is mostly co-localized with K8-positive cells throughout these stages (Supplementary Fig. 7d, e). This discordant result between CXCL12 mRNA and protein expression implies that CXCL12 is likely tightly regulated at both transcriptional and translational levels in different epithelial compartments during mammary gland development. Future research should delve into the intricate molecular mechanisms responsible for the observed disparity between low mRNA and high protein levels of CXCL12 in luminal cells, in contrast with the reverse pattern in basal cells.

These findings suggest that luminal epithelial cells are the major sources of CXCL12, which recruits macrophage to mammary epithelium to promote the MaSC capacity of basal epithelial cells. To investigate the role of luminal-CXCL12 on mammary gland development, we generated luminal epithelial cell-specific CXCL12 conditional knockout

https://doi.org/10.1038/s41467-025-59972-z

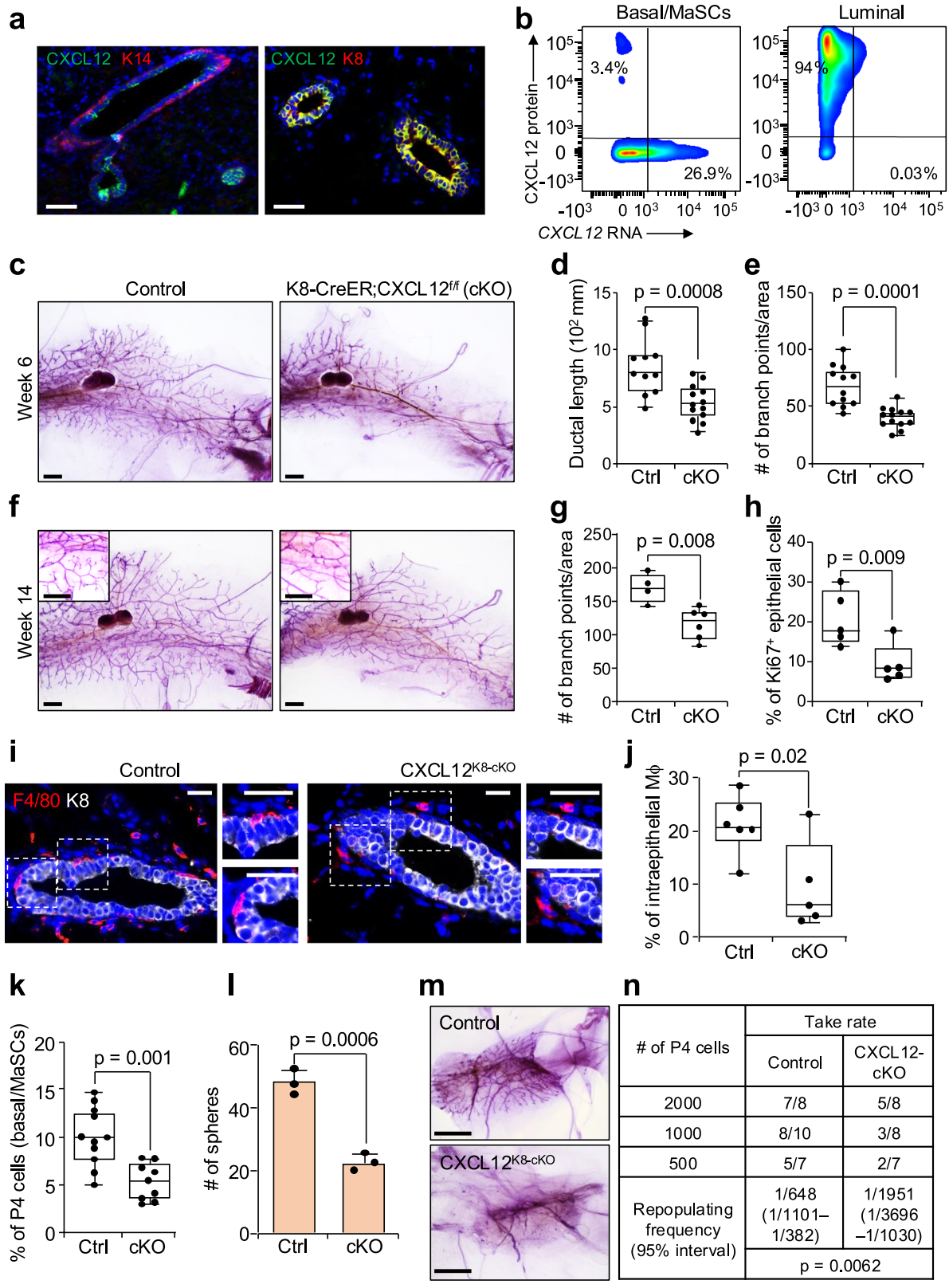

# of P4 cells	Take rate	
	Control	CXCL12-cKO
2000	7/8	5/8
1000	8/10	3/8
500	5/7	2/7
Repopulating frequency (95% interval)	1/648 (1/1101–1/382)	1/1951 (1/3696–1/1030)
	p = 0.0062	

mice (CXCL12$^{K8\text{-}cKO}$) by crossing CXCL12 floxed mice[57] with mice expressing luminal-specific K8-CreER[12]. A significantly reduced CXCL12 expression in luminal mammary epithelial cells of CXCL12$^{K8\text{-}cKO}$ mice was validated by qPCR and flow cytometry assay, while CXCL12 expression in basal cells remained unchanged (Supplementary Fig. 8a–c). Notably, we observed a delay of mammary gland development in CXCL12$^{K8\text{-}cKO}$ mice, with a significantly reduced mammary ductal length and branching at 6 weeks of age, and tertiary branching at 14 weeks compared to the control mice (Fig. 3c–g). In contrast, basal-specific CXCL12 conditional knockout (CXCL12$^{K14\text{-}cKO}$) mice showed only a statistically insignificant moderate reduction in both ductal elongation and branching formation (Supplementary Fig. 9a–f), suggesting a non-essential role of basal cells as the source of CXCL12 during mammary gland development. Immunofluorescent staining of

Fig. 3 | CXCL12 is mainly produced by luminal epithelial cells and is required for mammary ductal morphogenesis. a IF images of CXCL12 with Keratin 14 (K14) or Keratin 8 (K8) in WT mammary epithelium. **b** Representative flow cytometry plots showing CXCL12 protein and mRNA expression in basal/MaSCs and luminal cells. **c**, **f** Representative carmine alum-stained mammary glands from K8-CreER control (Ctrl) and CXCL12$^{K8\text{-}cKO}$ (cKO) mice at 6 and 14 weeks. **d**, **e**, and **g** Quantification of ductal length (**d**), and branching (**e** and **g**) in week 6 ($n = 10, 14$) and week 14 ($n = 4$, 6, biologically independent samples) mammary glands. **h** Quantification of Ki67+ epithelial cell in control vs. CXCL12$^{K8\text{-}cKO}$ mammary glands ($n = 4, 5$, biologically independent samples). **i** F4/80 and K8 IF staining of control and CXCL12$^{K8\text{-}cKO}$ mammary glands. Right panels show enlarged boxed regions. **j** Quantification of intraepithelial F4/80^{+} cell per field ($n = 3$, biologically independent samples, 2–3 ductal areas were randomly selected per each gland section for quantification). **k** Flow cytometry quantification of Lin^{-}CD24^{+}CD29^{Hi} P4 cells (basal/MaSCs) (Supplementary Fig. 16a) in control and CXCL12$^{K8\text{-}cKO}$ mammary glands ($n = 9, 11$, biologically independent samples). **l** Mammosphere formation assay with 5000 P4 cell from control and CXCL12$^{K8\text{-}cKO}$ ($n = 3$, biologically independent samples). **m**, **n** Limited dilution assay with basal/MaSCs from control and CXCL12$^{K8\text{-}cKO}$ mammary glands. Representative mammary outgrowths. Table representing serial dilution injections with the corresponding take rate and repopulation frequencies (calculated by ELDA, Pearson's Chi-squared test, two-sided). Scale bar, 50 µm (**a** and **i**), 25 µm (**c**, **f**, and **m**). Data are shown as mean values ± s.d. Statistical significance was calculated by two-tailed unpaired Student's *t*-test or one-way ANOVA with Turkey's test. Box plots show the median (center line), with box bounds representing the 25th and 75th percentiles (lower and upper quartiles). Whiskers extend to the most extreme values within 1.5x the interquartile range (IQR); points beyond this range are plotted as outliers. Source data are provided as a Source Data file.

Ki67 further revealed a significant decrease in proliferating mammary epithelial cells in CXCL12$^{K8\text{-}cKO}$ mice (Fig. 3h and Supplementary Fig. 8d), mirroring the phenotype of CXCR4$^{M\Phi\text{-}CKO}$ mice (Fig. 1l, m). Altogether, these results indicate that chemokine CXCL12 is mainly produced by luminal cells, and is pivotal to ductal branching morphogenesis during mammary gland development.

Luminal cell-derived CXCL12 is essential for the interaction of MaSCs with macrophages to create a stem cell-promoting niche

The abnormal mammary gland development shown in CXCL12$^{K8\text{-}cKO}$ mice could be due to the lack of MaSC-supporting macrophages within the epithelial niche. To test this possibility, we first measured the number of total and CXCR4-expressing macrophages in the mammary gland by flow cytometry analysis. The result showed a significantly reduced number of both total and CXCR4-expressing macrophages in the mammary glands of CXCL12$^{K8\text{-}cKO}$ mice, compared to control mice at both 6 and 14 weeks after birth (Supplementary Fig. 8e–h). No such defect was observed in CXCL12$^{K14\text{-}cKO}$ mice (Supplementary Fig. 9g). To test the possible impact of luminal CXCL12 depletion on CXCR4-expressing non-macrophage cells within the mammary glands, we measured the levels of CXCR4 in epithelial cells isolated from CXCL12$^{K8\text{-}cKO}$ mouse mammary glands. CXCR4 levels remained unchanged in basal cells and showed a moderate, statistically insignificant increase in luminal cells (Supplementary Fig. 8i). We further observed that luminal CXCL12 depletion did not alter the numbers of lymphoid cells, including CD8^{+}T, CD4^{+}T, NK and B cells, nor did it affect CXCR4 expression on B cells (Supplementary Fig. 8j, k). These data provide evidence that luminal CXCL12 primarily acts on CXCR4^{+} macrophages. Using immunofluorescent staining of F4/80 in the mammary gland of control and CXCL12$^{K8\text{-}cKO}$ mice, we observed a lack of the close association of macrophages with mammary ducts in CXCL12$^{K8\text{-}cKO}$ mice, similar to what we observed in CXCR4$^{M\Phi\text{-}cKO}$ mice (Fig. 3i, j). Next, we performed in vitro transwell assay to further evaluate migration properties of macrophages and observed reduced migratory ability of macrophages from CXCL12$^{K8\text{-}cKO}$ mice compared to controls (Supplementary Fig. 8l). The number of migrated cells was significantly increased with treatment of recombinant CXCL12 or in the presence of CXCL12-expressing luminal cells, and this effect was diminished when AMD3100, an inhibitor of CXCL12–CXCR4 signaling was added (Supplementary Fig. 8m, n). Supporting these findings, gene ontology pathway analysis showed that migration and chemotaxis-related pathways were highly upregulated in mammary macrophages from control mice compared to those from CXCL12$^{K8\text{-}cKO}$ mice (Supplementary Fig. 10a). GSEA further confirmed that enrichment of macrophage-specific chemotaxis and migration gene sets in mammary macrophages derived from control mice compared to those from CXCL12$^{K8\text{-}cKO}$ mice (Supplementary Fig. 10b).

These results indicate that CXCL12 produced by luminal cells is essential for the recruitment of ductal macrophages, which we have previously shown to provide critical niche signals to support the MaSC activity of basal cells[23]. Therefore, we investigated whether a delayed mammary ductal elongation and branching in CXCL12$^{K8\text{-}cKO}$ mice is due to a reduction in MaSC number or activity. We observed a significantly reduced number of Lin^{-}CD24^{+}CD29^{high} (P4) MaSC-enriched basal population in CXCL12$^{K8\text{-}cKO}$ mice (Fig. 3k). Furthermore, FACS-isolated P4 populations from CXCL12$^{K8\text{-}cKO}$ mice formed significantly fewer mammospheres in vitro, compared to cells from control mice (Fig. 3l). We further performed limiting dilution cleared fat pad reconstitution assay and revealed that CXCL12$^{K8\text{-}cKO}$ mice-derived P4 basal cells showed a significantly decreased repopulating ability (Fig. 3m and n). Taken together, these results indicate reduced MaSC properties of basal cells in mice lacking luminal expression of CXCL12.

To understand molecular features associated with diminished MaSC function in CXCL12$^{K8\text{-}cKO}$ mice, we isolated P4 cells from control and CXCL12$^{K8\text{-}cKO}$ mammary glands by FACS for RNA sequencing. GSEA indicated enrichments of Wnt activity and MaSC gene signature in P4 cells from controls versus CXCL12$^{K8\text{-}cKO}$ mice. Conversely, Wnt and β-catenin downregulated genes as well as luminal signatures were enriched in P4 cells from CXCL12$^{K8\text{-}cKO}$ mammary glands (Supplementary Fig. 10c). qRT-PCR analysis confirmed downregulation of several stem cell transcription factors and markers in P4 basal cells of CXCL12$^{K8\text{-}cKO}$ mammary gland (Supplementary Fig. 10d), similar to the decreased expression of these genes in P4 cells from CXCR4$^{M\Phi\text{-}cKO}$ mice (Supplementary Fig. 6c). Overall, there is marked similarity in both cellular phenotype and gene expression changes between CXCR4$^{M\Phi\text{-}cKO}$ and CXCL12$^{K8\text{-}cKO}$ -derived macrophages and P4 cells. This finding suggested that CXCR4 activation in macrophages is likely triggered by luminal cell-derived CXCL12. Such CXCL12–CXCR4 signaling axis in the macrophageal niche plays a critical role in sustaining Wnt-dependent regenerative activity of basal cells in the mammary gland.

CXCL12/CXCR4-AKT-β-catenin signaling cascade activates the migratory activity of mammary gland macrophages and supports a macrophageal niche for MaSCs

Our data provide evidence supporting the role of a CXCL12–CXCR4-mediated signaling cascade in facilitating interactions among macrophages, luminal, and basal cells, which leads to the formation of a localized niche that supports MaSC functions. CXCL12 is known to induce several downstream signaling events, including the PI3K-AKT and MAPK signaling pathways, primarily through the mediation of G protein-coupled receptors (GPCR)[58]. Furthermore, it exerts a variety of regulatory effects on cells in both physiological and pathological contexts[59,60]. To explore the molecular impact of CXCL12–CXCR4 signaling on mammary gland macrophages, we performed RNA sequencing of in vitro culturing of mammary gland-derived macrophages with or without treatment of recombinant CXCL12. Gene set enrichment analysis indicated elevated activity of Wnt and Notch pathways in mammary gland-derived macrophages upon CXCL12 stimulation (Fig. 4a and Supplementary Fig. 11a). Consistent with in vitro CXCL12 treatment effects on mammary

macrophages, both AKT and Wnt/β-catenin signaling were among the most enriched pathways in mammary gland macrophages from control mice compared to those from CXCL12$^{K8\text{-}cKO}$ mice (Supplementary Fig. 11b). Similarly, these pathways, including PI3K-Akt, Wnt, and Notch signaling, were found as the enriched pathways in CXCR4^{+} macrophages compared to CXCR4^{-} macrophages (Supplementary Fig. 11c). The roles of Wnt/β-catenin signaling in regulating macrophage polarization, proliferation and activity have been reported previously[61,62]. Therefore, we hypothesized that CXCL12 binding on CXCR4 induces AKT-mediated β-catenin stabilization and promotes its transcriptional activity in the mammary gland macrophages. Given that activated AKT stabilizes β-catenin via phosphorylation and inactivation of GSK3β and/or direct phosphorylation of β-catenin at Ser^{552}, leading to nuclear translocation of β-catenin and promotion of target gene transcription[63–65] (Supplementary Fig. 11d), the expression of activated AKT and different forms of β-catenin was first accessed by flow cytometry analysis. We detected a higher level of phosphorylated-AKT (pAKT) and phosphorylated-β-catenin at Ser^{552} (p-β-catenin) in CXCR4^{+} macrophages, compared with CXCR4^{-} cells (Fig. 4b, c). A higher expression of active β-catenin without GSK3β-mediated phosphorylation at Ser$^{33/37}$ was also observed in CXCR4^{+} macrophages (Supplementary Fig. 11e, f). In vitro, the expression of pAKT and p-β-catenin at Ser^{552} was increased in mammary gland-derived macrophages after recombinant CXCL12 treatment, and this was significantly blocked with an AKT inhibitor, GSK690693, and a CXCR4 inhibitor, AMD3100 (Fig. 4d–g, Supplementary Fig. 12a–c). Immunofluorescent imagining confirmed the nuclear expression of p-β-catenin at Ser^{552} in the macrophages surrounding the mammary epithelium. In contrast, macrophages in the mammary gland of CXCL12$^{K8\text{-}cKO}$ and CXCR4$^{M\Phi\text{-}cKO}$ mice showed the absence of nuclear p-β-catenin expression as well as reduced epithelial association (Fig. 4h).

Next, we evaluated the impact of the CXCL12–CXCR4–AKT pathway on Wnt/β-catenin target genes. Mammary gland-derived macrophages were pre-treated with an AKT inhibitor, GSK690693, prior to CXCL12 stimulation and subsequently subjected to RNA sequencing analysis. CXCL12 treatment stimulated the expression of Wnt/β-catenin target genes which are essential to cell survival (e.g. *Birc5/Survivin* and *Cdc25a*), proliferation (e.g. *Ccnd2* and *Ccnd3*) and migration (e.g. *Mmp2*, *Mmp12*, *Mmp13*), and this was diminished when combined with AKT inhibitor treatment (Fig. 5a, b). GSEA performed on mammary gland macrophages cultured with recombinant CXCL12 only or in combination with AKT inhibitor further confirmed that blocking of AKT signaling significantly downregulated gene signatures related to β-catenin transactivation, cell proliferation and ECM responses which is induced by CXCL12 stimulation (Supplementary Fig. 12d). The expression of several Wnt/β-catenin targets was validated by flow cytometry analysis, which showed a higher protein levels of WNT2b, CCND3, and MMP2 in CXCR4-positive macrophages, compared with CXCR4-negative cells (Fig. 5c, d).

A previous study identified Lyve-1^{+} mammary gland macrophages which are associated with the extracellular matrix (ECM)-rich mammary stroma[66], suggesting that macrophages may be involved in ECM remodeling during mammary gland development. Here, we observed the breach of the basement membrane (Fig. 1e) by mammary ductal macrophages to form direct cellular contact with the epithelial cells and induce juxtracrine stem cell niche signaling[23,39,67]. This indicated increased ability of ductal macrophage in ECM remodeling and invasion through the basement membrane. Indeed, expression of several proteases in mammary gland macrophages was induced upon CXCL12 treatment, and such increase was abolished by AKT inhibitor GSK690693 (Fig. 5a). To functionally evaluate the invasive ability of mammary gland macrophage, we performed in vitro invadopodia assay with macrophages pre-treated with recombinant CXCL12 and AKT inhibitor. Invadopodia are actin-rich protrusions associated with the degradation of the basement membrane[68]. We observed stimulation of invadopodia formation of mammary gland-derived macrophages (Fig. 5e), as indicated by increased degraded gelatin in the presence of recombinant CXCL12 (Fig. 5f, g). AKT inhibitor (GSK) treatment resulted in significantly decreased invasive ability of macrophages (Fig. 5e–g). MMP2 has been identified as one of the invadopodia-relevant MMP isoforms[68]. We detected increased expression of MMP2 in the mammary gland macrophages after CXCL12 treatment, and this was blocked with the AKT inhibitor (Fig. 5a, Supplementary Fig. 12e and f).

We and others have previously identified various sources of niche Wnts, including hormone receptor-positive luminal cells, basal cells, and tissue-resident macrophages[23,69–72]. To validate the functional importance of Wnts produced by luminal cells and macrophages on MaSC activity, we performed an in vitro mammosphere co-culture experiment using transwell systems. The results showed enhanced mammosphere formation of MaSC/basal cells when co-cultured with either luminal cells or macrophages, with this effect further increased in the presence of both cell types. Treatment with a Wnt signaling inhibitor, ICG-001, eliminated the ability of both luminal cells and macrophages to promote mammosphere formation under these co-culture conditions (Supplementary Fig. 12g). These findings highlight the critical role of both epithelial and macrophages-derived Wnts in supporting the MaSC activity of basal cells. In the current study, we further found that the CXCL12–AKT pathway stimulates the expression of Wnt ligands, such as Wnt2b, in CXCR4-positive macrophages (Fig. 5b–d), which may play a role in regulating MaSC activity. Immunofluorescent staining confirmed abundant expression of WNT2b in ductal macrophages within the mammary epithelium (Fig. 5h). Next, we sought to directly assess the role of the AKT-β-catenin signaling cascade in mediating the MaSC-promoting function of CXCR4^{+} mammary gland macrophage stimulated by CXCL12. To this end, MaSC-enriched P4 basal cells were co-cultured with mammary gland-derived macrophages pre-treated with or without recombinant CXCL12 and AKT inhibitor. The results showed enhanced mammosphere formation of P4 cells by CXCL12 primed-mammary gland macrophages and this was significantly diminished by the presence of an AKT inhibitor (Fig. 5i).

CXCR4^{+} mammary gland macrophages promote mammary tumor initiation and progression in multiple models

Similar to MaSCs that interact with a specialized niche and niche-associated signals during normal development, breast tumor-initiating cells (TICs) are influenced by various niche factors and stromal cells within a specific tumor-initiating niche, promoting malignant progression[4,73,74]. For example, in a Trp53 null mouse model of basal-like breast cancer, it has been previously reported that heterogeneous populations of tumor cells co-exist within the same tumor, with CXCL12-expressing tumor cells supporting the TIC activity of CXCR4^{+} TICs[75]. However, it remains largely unknown which specific stromal cell types exist in the niche and how they support TICs. After identifying a unique population of CXCR4^{+} mammary gland macrophages that supports MaSCs via the CXCL12–CXCR4–AKT–β-catenin signaling cascade, we sought to determine whether the identical macrophageal niche and its associated signals also contribute to promoting TIC activity during mammary tumorigenesis. To this end, we first examined the presence of CXCR4^{+} macrophages during mammary tumorigenesis. Flow cytometry analysis revealed a significant increase in CXCR4^{+}F4/80^{+}CD11b^{+} macrophages during the progression from normal glands to preneoplasia lesions and tumors in the MMTV-PyMT model, which represent the luminal subtype of mammary gland tumors[76] (Fig. 6a, b). IF imaging of FFPE tissue sections from PyMT mice indicated that CXCR4-expressing macrophages localized near preneoplasia glands and tumors (Fig. 6c and Supplementary Fig. 13a). We next sought to determine the cellular source of CXCL12 in preneoplasia glands and early tumors, which may contribute to the

https://doi.org/10.1038/s41467-025-59972-z

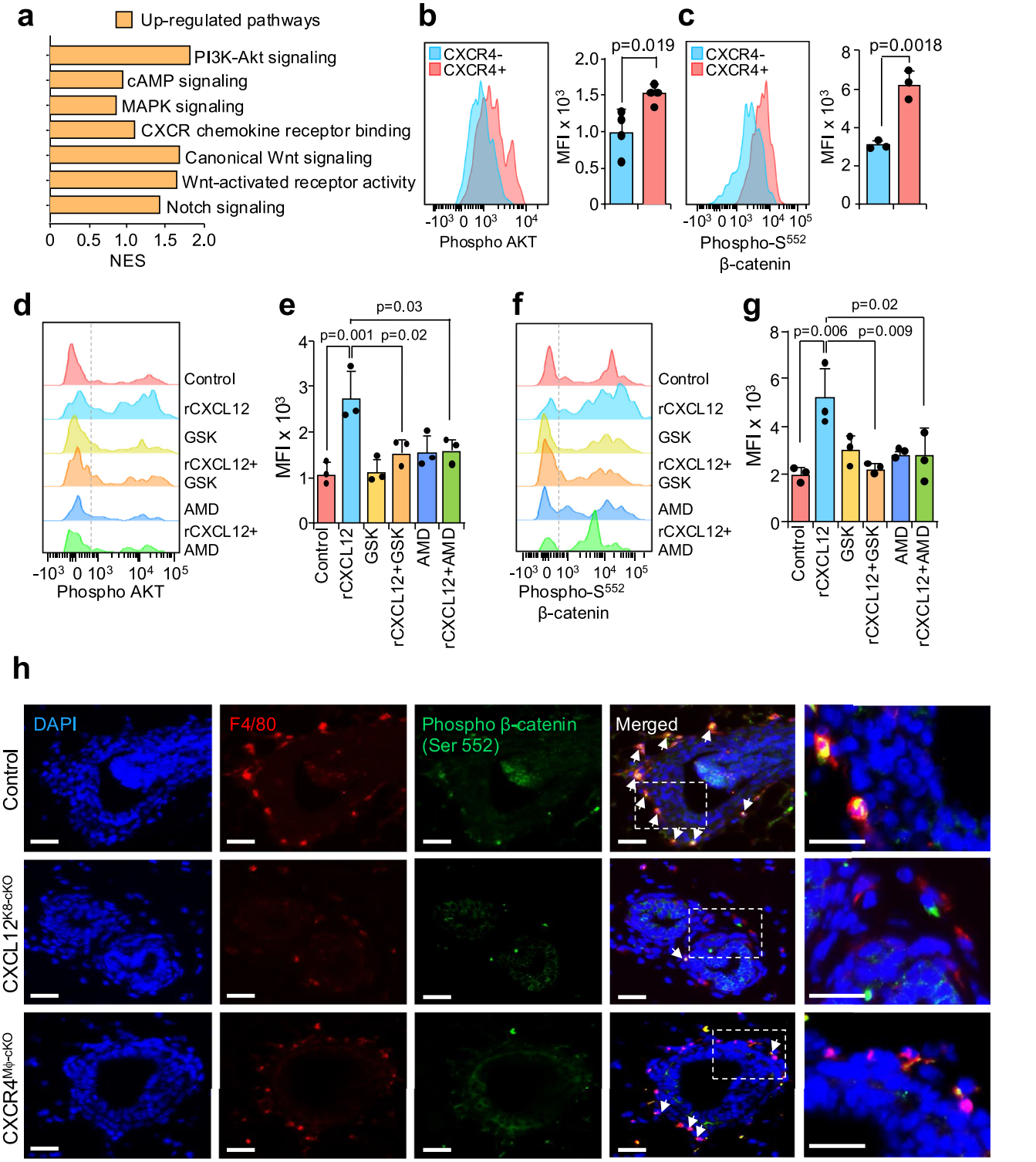

Fig. 4 | CXCL12–CXCR4 axis induces AKT-mediated β-catenin activation in CXCR4⁺ mammary gland macrophages. a Pathway enrichment analysis from differentially expressed genes in CXCL12-treated versus non-treated control Mϕ. **b**, **c** Flow cytometry histogram presentation of the expression and mean fluorescent intensity (MFI) of phosphorylated-AKT (**b**) and phosphorylated-β-catenin (Ser^{552}) (**c**) in CXCR4^{+} and CXCR4^{-} mammary gland macrophages ($n = 4, 3$, biologically independent samples). **d**, **f** Flow cytometry histogram presentation of the expression of phosphorylated-AKT (**d**) and phosphorylated-β-catenin (Ser^{552}) (**f**) in mammary gland macrophages cultured in vitro with 200 ng/ml recombinant CXCL12 (rCXCL12), 10 μM AKT inhibitor, GSK690693 (GSK) and 10 μM CXCR4 inhibitor AMD3100 (AMD). **e**, **g** MFI of phosphorylated-AKT (**e**) and phosphorylated-β-catenin (Ser^{552}) (**g**) in macrophages with different treatment conditions measured by flow cytometry analysis ($n = 3$, biologically independent samples). **h** IF co-staining of F4/80 with phosphorylated-β-catenin (Ser^{552}) in littermate control, CXCL12$^{K8\text{-}cKO}$ and CXCR4$^{Mϕ\text{-}cKO}$ mammary glands. The enlargement of areas marked by dashed line boxes is shown on the right panels. White arrows indicated double-positive cells. Scale bar, 50 μm in (**h**). Flow cytometry analysis of Mϕ gate (Supplementary Fig. 16b) for MFI quantification in (**b**–**g**). Data are presented as mean values ± s.d. Statistical significance was calculated by two-tailed unpaired Student's *t*-test or one-way ANOVA with Turkey's multiple comparisons test. Source data are provided as a Source Data file.

https://doi.org/10.1038/s41467-025-59972-z

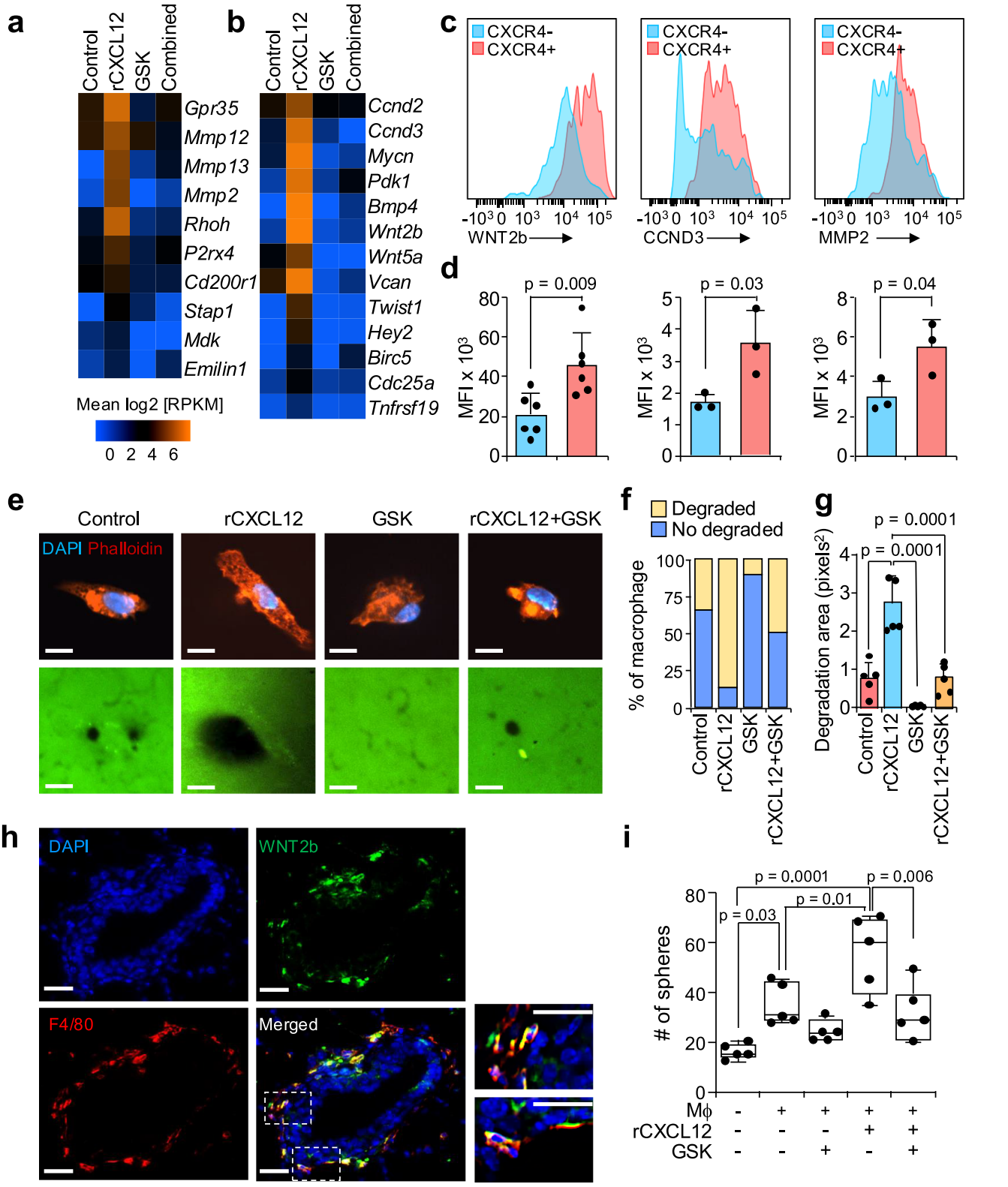

increased frequency of CXCR4⁺ macrophages during tumorigenesis. Flow cytometry analysis revealed that while HR⁺ luminal cells are the primary source of CXCL12 in the normal mammary gland, CXCL12 levels are significantly elevated in basal cells, luminal progenitors (LP), and smooth muscle actin (SMA)-positive fibroblasts during tumor progression. It is notable that SMA⁺ cancer-associated fibroblasts (CAFs) have been previously identified as a key cellular source of CXCL12 in cancer[77], which is consistent with our findings (Supplementary Fig. 13b).

To investigate the importance of CXCR4⁺ macrophages during autochthonous mammary tumor progression, we crossed CXCR4$^{Mϕ\text{-}cKO}$ mice with MMTV-PyMT mice to generate PyMT;CXCR4$^{Mϕ\text{-}cKO}$ animals. Significantly reduced CXCR4 expression in the macrophages of these knockout mice was confirmed by flow cytometry assay while the

Fig. 5 | CXCL12/CXCR4–AKT–β-catenin signaling induces invasive and MaSC-promoting activity of CXCR4⁺ mammary gland macrophages. a, **b** Heatmaps showing differentially expressed genes related to Wnt/β-catenin pathways from RNA seq analysis of mammary gland-derived macrophages cultured with recombinant CXCL12 (rCXCL12) or AKT inhibitor GSK690693 (GSK), or both. **c** Flow cytometry histogram presentation of the expression of Wnt2b, CCND3, and MMP2 in CXCR4⁺ and CXCR4⁻ mammary gland macrophages (Supplementary Fig. 16b). **d** MFI of Wnt2b, CCND3, and MMP2 in macrophages measured by flow cytometry analysis ($n = 6, 3, 3$ per each group, biologically independent samples). **e** Representative images of mammary gland-derived macrophages forming invadopodia stained with DAPI and Phalloidin (red), and images of fluorescein-gelatin (green—on the bottom) **f**, **g** Quantification of invadopodia formation ability measured by (**f**) the percentage of the macrophages that co-localize with degraded versus non-degraded gelatin area and (**g**) the size of gelatin degradation in a defined area ($n = 5$, biologically independent samples). **h** IF co-staining of F4/80 with Wnt2b in WT mammary glands. Enlargement of areas marked by dashed line boxes is shown at the right panels. **i**, Quantification of mammosphere formation assay with 5000 P4 cells from WT cocultured with 20,000 macrophages pre-treated with recombinant CXCL12 and AKT inhibitor ($n = 5$, biologically independent samples). Scale bar, 10 μm in (**e**) and 50 μm in (**h**). Data are presented as mean values ± s.d. Statistical significance was calculated by two-tailed unpaired Student's *t*-test or one-way ANOVA with Turkey's multiple comparisons test. Box plots show the median (center line), with box bounds representing the 25th and 75th percentiles (lower and upper quartiles). Whiskers extend to the most extreme values within 1.5× the interquartile range (IQR); points beyond this range are plotted as outliers. Source data are provided as a Source Data file.

percentage of total F4/80⁺CD11b⁺ macrophages remained unaffected (Supplementary Fig. 13c–e). We observed a significant delay in tumor onset in PyMT;CXCR4$^{Mϕ\text{-}cKO}$. The average age of tumor occurrence in the control littermate group was about 90 days, consistent with previous reported average latency of 92 days of PyMT mammary tumors in the C57BL/6J background[78,79], whereas the PyMT;CXCR4$^{Mϕ\text{-}cKO}$ group developed tumors after 112 days (Fig. 6d). We also found delayed primary tumor growth and suppressed lung metastasis in PyMT;CXCR4$^{Mϕ\text{-}cKO}$ mice (Fig. 6e, f). The whole mounts and hematoxylin and eosin-staining sections of mammary glands at 10 weeks of preneoplastic stage showed that PyMT;CXCR4$^{Mϕ\text{-}cKO}$ glands exhibited fewer and smaller hyperplasia foci mingled with normal ductal structures compared to expensive hyperplasia in the glands of PyMT littermate control (Fig. 6g and Supplementary Fig. 13f). These results indicate the contribution of mammary tissue-resident CXCR4⁺ macrophages to early PyMT tumorigenesis.

We next examined the composition of mammary epithelial cells (MECs) in preneoplastic glands using CD24, CD29, and CD61, which are commonly used to identify luminal and basal MEC subsets[8,80]. Compared to littermate PyMT controls, the percentage of CD24⁺CD29^{low}CD61⁺ luminal progenitors (LPs) significantly decreased in PyMT;CXCR4$^{Mϕ\text{-}cKO}$ preneoplastic glands. In contrast, basal cells remained unchanged, and total luminal cells showed a moderate reduction in PyMT;CXCR4$^{Mϕ\text{-}cKO}$ mice (Fig. 6h–j). It is noteworthy that a lower number of LP was also observed in the normal non-tumor bearing mammary glands of CXCR4$^{Mϕ\text{-}cKO}$ mice compared to controls, suggesting a conserved role of CXCR4⁺ macrophages in LP survival and maintenance during tissue homeostasis and tumorigenesis (Supplementary Fig. 13g).

Previous transcriptomic analysis has reported luminal progenitors as the cell of origin of PyMT tumors[81,82] and they are expanded during tumorigenesis[83,84]. This result suggests a functional role for CXCR4⁺ macrophages in supporting the expansion of PyMT TICs. To further test whether CXCR4 depletion in macrophages influences the tumor-initiating properties of TICs, we sorted either MECs or LPs from PyMT control and PyMT;CXCR4$^{Mϕ\text{-}cKO}$ preneoplastic glands to assess tumor-forming capacity using in vitro tumorsphere formation and in vivo limited dilution tumorigenesis assay. We also isolated LPs from wild-type and CXCR4$^{Mϕ\text{-}cKO}$ mice to evaluate their mammosphere-forming ability. In contrast to similar mammosphere forming ability of LPs from normal mammary glands of control and CXCR4$^{Mϕ\text{-}cKO}$ mice (Supplementary Fig. 13h), LPs from preneoplastic glands of CXCR4$^{Mϕ\text{-}cKO}$ mice formed significantly fewer tumorspheres in vitro compared to those from control mice (Supplementary Fig. 13i), suggesting a higher dependence of LP activity on CXCR4⁺ macrophages after oncogenic transformation. We also co-cultured MECs with CXCR4⁺ or CXCR4⁻ macrophages and found that the CXCR4⁺ macrophages exhibited significantly greater efficacy in stimulating the tumorsphere-forming capacity of MECs (Fig. 7a). Moreover when MECs or LPs isolated from wild-type PyMT preneoplastic glands were orthotopically transplanted into controls and CXCR4$^{Mϕ\text{-}cKO}$ mice, we observed significantly reduced incidence and volumes of tumors grown in CXCR4$^{Mϕ\text{-}cKO}$ recipients (Fig. 7b and c and Supplementary Fig. 13j and k). These results suggest that a CXCR4-deficient macrophageal niche could not sufficiently support the tumorigenic potential as well as the expansion of TICs during tumorigenesis.

We next sought to validate the tumor-initiating properties of CXCR4⁺ niche macrophages in the MMTV-Wnt model, which produces basal-like mammary tumors, as well as the allograft models using luminal B cancer-like E0771[85] and the basal/TNBC (triple-negative breast cancer)-like Py8119[86]. Compared to Wnt littermate controls, Wnt;CXCR4$^{Mϕ\text{-}cKO}$ mice also showed significantly delayed tumor onsets (Fig. 7d). We conducted an in vivo limited dilution tumorigenesis assay by injecting wild-type Wnt MECs into controls and CXCR4$^{Mϕ\text{-}cKO}$ mice, and observed reduced tumor incidence and volume in the CXCR4$^{Mϕ\text{-}cKO}$ recipients (Fig. 7e, f). These phenotypes closely resembled those observed in the MMTV-PyMT tumor model. Next, two allograft models were employed for further validation. We orthotopically implanted E0771 and Py8119 mouse mammary tumor cell lines into control and CXCR4$^{Mϕ\text{-}cKO}$ mice. While significantly delayed primary tumor growth was observed only in E0771-injected CXCR4$^{Mϕ\text{-}cKO}$ mice, both E0771 and Py8119 tumor-bearing CXCR4$^{Mϕ\text{-}cKO}$ mice showed significantly suppressed lung metastasis (Supplementary Fig. 13l–q).

To characterize the molecular features of control and CXCR4$^{Mϕ\text{-}cKO}$ macrophages derived from preneoplastic PyMT glands, we performed RNA sequencing analysis. GSEA revealed increased enrichment of gene signatures related with Notch and Wnt signaling in control macrophages compared to CXCR4$^{Mϕ\text{-}cKO}$ macrophages (Fig. 7g). Similarly, the expression of key Notch/Wnt genes, such as *Wnt2b*, *Wnt5b, Ccnd3, Mmp2, Mmp8*, and *Birc5* was reduced in macrophages derived from CXCR4$^{Mϕ\text{-}cKO}$ preneoplastic glands (Fig. 7h). We detected a higher level of pAKT, p-β-catenin at Ser^{552}, WNT2B, and MMP2 in PyMT-derived CXCR4⁺ macrophages, compared with CXCR4⁻ cells (Fig. 7i). In addition, tumorsphere assay with PyMT MECs co-cultured with macrophages pre-treated with recombinant CXCL12, or combined with CXCR4, Akt, and Wnt inhibitors, demonstrated that CXCL12 primed-macrophages enhanced tumorsphere formation of TICs and this effect was significantly diminished by the presence of these inhibitors (Fig. 7j). These results suggest that CXCR4 expression in preneoplasia niche macrophages promotes Akt/β-catenin/Wnt-dependent signaling, which is required to sustain TIC activity, similar to its role in maintaining MaSCs during normal development.

CXCR4⁺ mammary gland macrophages facilitate the formation of an early immunosuppressive niche by inducing regulatory T cells

Gene expression profiling also revealed that macrophages derived from preneoplasia glands showed enrichment of immune-related signatures, including "Tumor escape from immune attack", "TNFα signaling via NFκB", and "Negative regulation of T cell receptor signaling" (Fig. 7g). This suggests that macrophage with CXCR4 expression may

https://doi.org/10.1038/s41467-025-59972-z

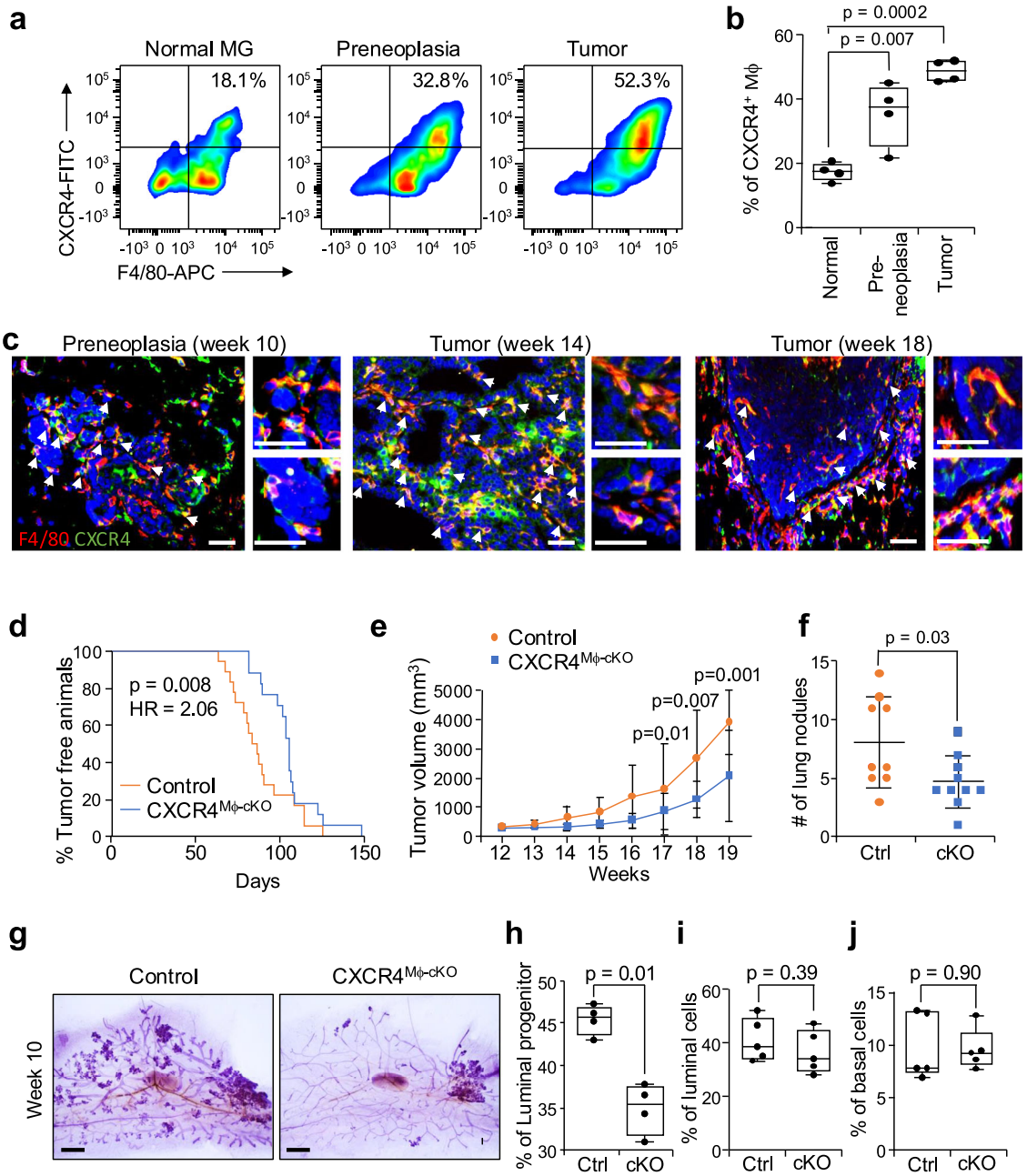

Fig. 6 | Genetic depletion of CXCR4 in mammary gland macrophage inhibits mammary tumorigenesis. a Representative flow cytometry plots showing the percentage of $CXCR4^+F4/80^+$ Mϕ among $CD11b^+$ cells from the normal mammary gland (MG) from 8-week-old wild-type female mice, preneoplasia glands from 10-week-old PyMT mice, and tumors from 18-week-old PyMT mice. **b** The percentage of $CXCR4^+F4/80^+CD11b^+$ Mϕ by flow cytometry analysis (Supplementary Fig. 16b) ($n = 4$, biologically independent samples). **c** IF images of cells co-stained with antibodies against CXCR4 (green) and F4/80 (red) in preneoplasia glands from 10-week-old PyMT mice, and tumors from 14- and 18-week-old PyMT mice. White arrows indicated double-positive cells. The enlargement of areas is shown on the right panels. **d** Kinetics of mammary tumor onset in PyMT;control ($n = 20$) and PyMT;$CXCR4^{Mϕ\text{-}cKO}$ mice ($n = 20$) as shown by Kaplan–Meier plot. *P* value by two-tailed log-rank test and hazard ratio (HR) measured. **e** Primary tumor growth rate of PyMT;control ($n = 9$, Ctrl) and PyMT;$CXCR4^{Mϕ\text{-}cKO}$ ($n = 9$, cKO) mice. **f** The number of lung metastasis in PyMT;control ($n = 9$) and PyMT;$CXCR4^{Mϕ\text{-}cKO}$ ($n = 9$) mice. **g** Carmine alum whole mount staining of preneoplastic glands from PyMT;control and PyMT;$CXCR4^{Mϕ\text{-}cKO}$ mice at 10 weeks. **h–j** Quantification of flow cytometry analysis (Supplementary Fig. 16a) showing the percentage of $Lin^-CD24^+CD29^{low}CD61^+$ cells (luminal progenitor, LP) (**h**), $Lin^-CD24^+CD29^{lo}$ luminal cells (**i**), and $Lin^-CD24^+CD29^{Hi}$ basal/MaSCs (**j**) from PyMT;control and PyMT;$CXCR4^{Mϕ\text{-}cKO}$ preneoplasia glands ($n = 4,5$ per each group, biologically independent samples). Scale bar, 50 μm in (**c**) and 25 μm in (**g**). Data are presented as mean values ± s.d. Statistical significance was calculated by two-tailed unpaired Student's *t*-test or one-way ANOVA with Turkey's multiple comparisons test. Box plots show the median (center line), with box bounds representing the 25th and 75th percentiles (lower and upper quartiles). Whiskers extend to the most extreme values within 1.5× the interquartile range (IQR); points beyond this range are plotted as outliers. Source data are provided as a Source Data file.

involve in regulating anti-tumor immune response in the early stages of tumorigenesis. Recent studies have shown that TICs develop unique immune-escape properties, driving malignant tumor growth and progression[87–89]. Given that solid cancers often originate from tissue-specific stem or progenitor cells that acquire oncogenic mutations and malignant traits[11,90–92], normal MaSCs and their niche components are likely co-opted during tumorigenesis to confer an immunosuppressive advantage to tumor cells.

https://doi.org/10.1038/s41467-025-59972-z

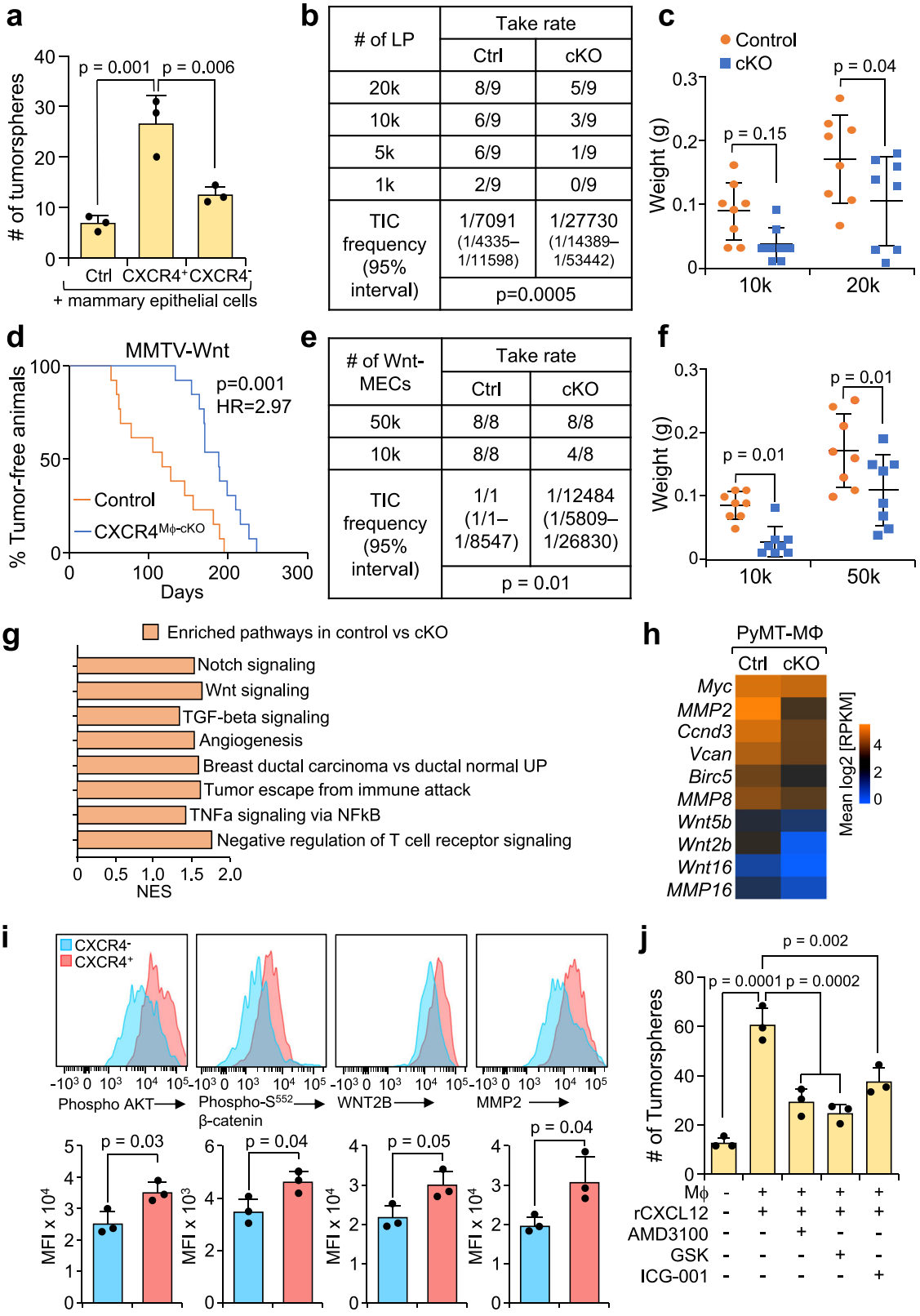

# of LP	Take rate	
	Ctrl	cKO
20k	8/9	5/9
10k	6/9	3/9
5k	6/9	1/9
1k	2/9	0/9
TIC frequency (95% interval)	1/7091 (1/4335–1/11598)	1/27730 (1/14389–1/53442)
	p=0.0005	

# of Wnt-MECs	Take rate	
	Ctrl	cKO
50k	8/8	8/8
10k	8/8	4/8
TIC frequency (95% interval)	1/1 (1/1–1/8547)	1/12484 (1/5809–1/26830)
	p = 0.01	

To gain molecular insights into the role of CXCR4^{+} macrophages in the tumor-initiating niche and their interactions with TICs and other immune components, we performed single-cell RNA sequencing of preneoplasia glands isolated from PyMT controls and PyMT;CXCR4$^{MΦ\text{-}cKO}$ mice (Supplementary Fig. 14a–d). We observed a decreased frequency of regulatory T cells (Treg) and an increased frequency of CD8^{+} T cells in PyMT;CXCR4$^{MΦ\text{-}cKO}$ preneoplasia glands compared with PyMT controls (Fig. 8a, b). It has been shown that Tregs protect various normal stem cells from immune attacks, effectively creating an immune-privileged niche[93,94]. In breast cancer, an increased frequency of Tregs is observed in ductal carcinoma in situ (DCIS) and is associated with its invasive progression[95,96]. Similarly, a study of early lung adenocarcinoma shows that Tregs are the major immune components, with a striking increase in tumor

Fig. 7 | Genetic depletion of CXCR4 in mammary gland macrophages inhibits TIC activity. a Tumorsphere formation assay using 5000 MECs co-cultured with and without 20,000 CXCR4$^+$ and CXCR4$^-$ macrophages from PyMT control preneoplastic glands ($n = 3$, biologically independent samples). **b** Limited dilution tumorigenesis assay with luminal progenitor (LP) cells from PyMT preneoplastic glands injected into LysM-Cre control (Ctrl) and CXCR4$^{Mϕ\text{-}cKO}$ (cKO) recipient mice. Table representing serial dilution injections with the corresponding take rate and repopulation frequencies (calculated by ELDA, Pearson's Chi-squared test, two-sided). **c** Tumor weights from PyMT LPs injected into LysM-Cre control ($n = 8$) or CXCR4$^{Mϕ\text{-}cKO}$ recipients ($n = 8$). **d** Kaplan–Meier curve showing tumor onset in MMTV-Wnt control ($n = 13$) and MMTV-WntT;CXCR4$^{Mϕ\text{-}cKO}$ ($n = 13$) mice; log-rank p-value and hazard ratio (HR) shown. **e** Limited dilution tumorigenesis assay using MECs from MMTV-Wnt preneoplastic glands injected into control and CXCR4$^{Mϕ\text{-}cKO}$ mice. Table representing serial dilution injections with the corresponding take rate and repopulation frequencies (calculated by ELDA, Pearson's Chi-squared test, two-sided). **f** Tumor weights from MMTV-Wnt MECs injected into control ($n = 8$) or CXCR4$^{Mϕ\text{-}cKO}$ recipient ($n = 8$) mice. **g** GSEA of pathways enriched in Mϕ from PyMT control vs. PyMT;CXCR4$^{Mϕ\text{-}cKO}$ mice. **h** Heatmap of differentially expressed Notch/Wnt-related genes from RNA-seq of PyMT control and PyMT;CXCR4$^{Mϕ\text{-}cKO}$ Mϕ. **i** Flow cytometry histograms showing expression and MFI of pAKT, p-β-catenin (Ser^{552}), WNT2B, and MMP2 in CXCR4$^+$ vs. CXCR4$^-$ PyMT preneoplastic gland Mϕ (Supplementary Fig. 16b) ($n = 3$, biologically independent samples). **j** Tumorsphere assay using 5000 MECs co-cultured with 20,000 Mϕ pre-treated with rCXCL12 (200 ng/ml), AMD3100 (10 μM), AKT inhibitor GSK690693 (GSK, 10 μM), or Wnt inhibitor, ICG-001 (20μM) ($n = 3$, biologically independent samples). Data are mean values ± s.d. Statistical analysis by two-tailed unpaired Student's t-test or one-way ANOVA with Turkey's test. Box plots show the median (center line), 25th/75th percentiles (box bounds), whiskers extending to 1.5× IQR, and outliers plotted individually. Source data are provided as a Source Data file.

lesions compared to adjacent healthy tissues[97]. These findings suggest that Tregs are crucial for facilitating early immune evasion, which is necessary for the maintenance and activity of TICs. Flow cytometry analysis confirmed fewer Tregs in PyMT;CXCR4$^{Mϕ\text{-}cKO}$ preneoplasia glands compared with controls (Fig. 8c, d). We also detected a significant reduction of Tregs in Py8119 tumors grown in the CXCR4$^{Mϕ\text{-}cKO}$ mice and in MMTV-WNT;CXCR4$^{Mϕ\text{-}cKO}$ preneoplasia glands (Supplementary Fig. 14e and f). Furthermore, flow cytometry analysis and IF staining revealed increased CD8 T cell infiltrations in PyMT;CXCR4$^{Mϕ\text{-}cKO}$ tumors (Fig. 8e and Supplementary Fig. 14g), consistent with scRNA-seq data. Moreover, differential expression analysis of cKO vs control CD8 T cells revealed increased expression of cytotoxic lymphocyte markers, such as *Gzma, Gzmb, Klrk1* and *Ifitm2*, in CD8 T cells from PyMT;CXCR4$^{Mϕ\text{-}cKO}$ sample (Fig. 8f), confirming that Treg-mediated suppression of anti-tumor immunity is diminished in PyMT;CXCR4$^{Mϕ\text{-}cKO}$ mice.

To examine whether CXCR4$^+$ macrophages directly regulate Treg differentiation, we conducted an in vitro Treg differentiation assay by co-culturing primary macrophages isolated from PyMT control and PyMT;CXCR4$^{Mϕ\text{-}cKO}$ preneoplasia glands with naïve T cells. While both types of macrophages induced Treg differentiation, the control macrophages exhibited significantly greater efficacy at promoting the differentiation of naïve T cells into Treg cells than CXCR4-depleted macrophages (Fig. 8g). We confirmed that CXCR4$^+$ macrophages have a greater capacity to induce the differentiation of Tregs compared to CXCR4$^-$ macrophages (Fig. 8h). We further tested whether CXCL12 stimulation could enhance macrophages' ability to promote Treg differentiation. Indeed, Treg induction was significantly increased when naïve T cells were co-cultured with CXCL12-primed macrophages, suggesting a direct effect of CXCL12 on Treg differentiation (Supplementary Data Fig. 14h).

We next sought to uncover the molecular mechanisms by which CXCR4$^+$ macrophages induce Tregs differentiation. Bulk RNA sequencing analysis comparing control versus CXCR4$^{Mϕ\text{-}cKO}$ macrophages revealed decreased expression of ALDH1a2, a key enzyme involved in retinoic acid (RA) biogenesis, in CXCR4$^{Mϕ\text{-}cKO}$ macrophages (Supplementary Fig. 14i). It has been reported that ALDH1a2-mediated RA production in dendritic cells promotes Treg differentiation[98,99], however its role in macrophage-mediated breast tumorigenesis and immune suppression remains largely unexplored. Flow cytometry analysis confirmed higher ALDH1a2 expression in CXCR4$^+$ macrophages derived from PyMT preneoplasia glands compared to CXCR4$^-$ macrophages (Supplementary Fig. 14j). Additionally, CXCR4 knockout in macrophages significantly decreased ALDH enzymatic activity in the Aldefluor assay (Supplementary Fig. 14k). To investigate the functional importance of ALDH1a2 in macrophage-mediating immune suppression, we utilized an ALDH1a2 inhibitor recently developed in our lab, KyA33 (US patent US12,162,855), to assess its efficacy in inhibiting Treg differentiation and tumorigenesis. We first validated that KyA33 significantly reduced ALDH enzymatic activity in control macrophages to a level similar to those in CXCR4$^{Mϕ\text{-}cKO}$ macrophages (Supplementary Fig. 14k). Importantly, we observed that KyA33 effectively suppressed macrophage-induced Treg differentiation in vitro (Supplementary Fig. 14l). Next, we tested the in vivo efficacy of KyA33 using a limited dilution tumorigenesis assay. PyMT MECs were injected into wild-type C57BL/6J mice, which were subsequently treated with KyA33 in their feed. KyA33 treatment resulted in a significant reduction in both tumor incidence and volume (Supplementary Fig. 14m–o). In vivo treatment of KyA33 also decreased the percentage of Tregs in the tumors (Supplementary Fig. 14p). Together, these findings demonstrate that elevated expression of ALDH1a2 in CXCR4$^+$ macrophages contributes to the increased ability of CXCR4$^+$ macrophages in promoting Treg differentiation and breast tumorigenesis. We also conducted pathway analysis with differentially expressed genes (DEGs) in luminal cells from control and CXCR4$^{Mϕ\text{-}cKO}$ mammary tumors. PyMT;CXCR4$^{Mϕ\text{-}cKO}$ luminal cells expressed distinct molecular features associated with the apoptotic process and immune response, whereas control cells expressed pathways related to tumor progressions, such as migration and angiogenesis (Supplementary Fig. 14q). Differential expression analysis revealed an increased expression of multiple interferon-related genes in luminal cells from PyMT;CXCR4$^{Mϕ\text{-}cKO}$ sample, while control cells expressed genes involved in tumorigenesis and progression (Supplementary Fig. 14r). Taken together, these results indicate that CXCR4$^+$ macrophages closely interact with tumor cells early during tumorigenesis, and promote Treg differentiation and infiltration, thereby protecting tumors from CD8$^+$ T cell-dependent anti-tumor immunity.

Next, we sought to determine whether pharmacological targeting of the CXCL12–CXCR4 axis could attenuate mammary tumor initiation and progression. To this end, MMTV-PyMT mice were treated with either distilled water (control) or AMD3100 (Plerixafor) in drinking water starting as early as 6 weeks of age for a long-term treatment procedure. Notably, we found significantly delayed tumor onset, primary tumor growth, and suppressed lung metastasis in PyMT mice with AMD3100 treatment (Fig. 8i–k). Flow cytometry analysis showed that AMD3100 treatment decreased the percentage of Tregs and luminal cells, while the number of CXCR4$^+$ macrophages remained unchanged (Supplementary Fig. 14s).

To explore the clinical significance of macrophage with CXCR4 expression in breast cancer, we performed bulk-RNA sequencing of whole preneoplasia gland cells isolated from PyMT control and PyMT;CXCR4$^{Mϕ\text{-}cKO}$ mice, and generated a gene signature with the top 30 DEGs in control vs CXCR4$^{Mϕ\text{-}cKO}$ samples. This CXCR4$^+$Mϕ-associated gene signature was then used to measure correlations with the overall survival of subtype-specific breast cancer patients from the KM plotter data set[100]. Kaplan–Meier plots of survival probability showed that high expression of the CXCR4$^+$ Mϕ gene signature is associated with poor survival in breast cancer patients,

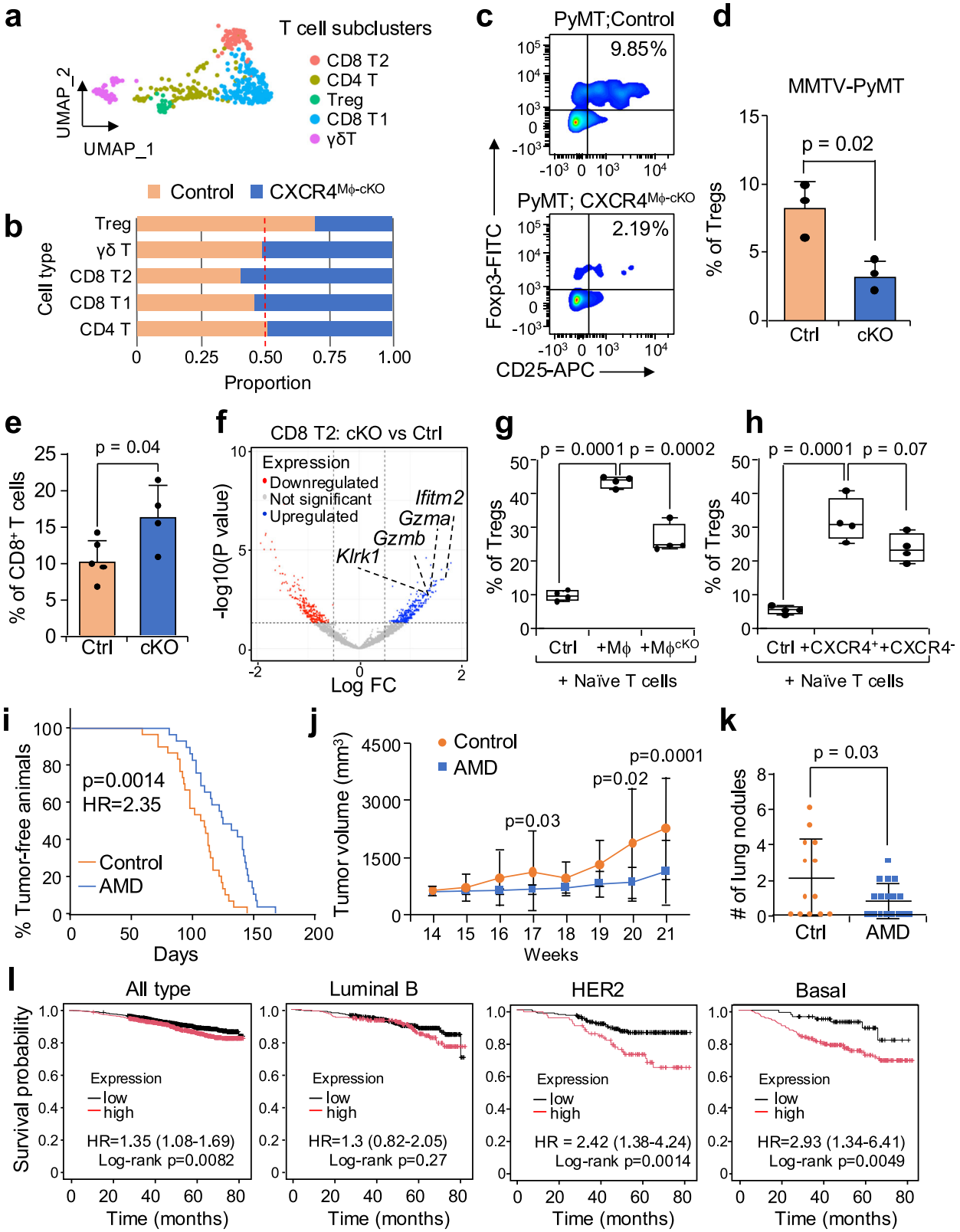

especially in HER2-positive and basal subtypes of breast cancers (Fig. 8l).

Discussion

In the study of adult stem cell systems, defining a specific niche population and its relevant functional mechanisms often represents a major advance in our understanding of how normal and cancerous stem cells interact with their surrounding niches and benefit from such interactions. Examples of such landmark discoveries include the identification of CXCL12-abundant reticular cells (CAR) as key components of perivascular niche for hematopoietic stem cells (HSCs)[57,101,102], CD81+PDGFRAlow, and RSPO3+GREM1+ fibroblasts as niche cells for intestinal stem cells (ISCs)[103,104], CD10+GPR77+ CAFs as part of cancer stem cell niche[105] and STAT3+ astrocytes as drivers of

Fig. 8 | CXCR4$^+$ macrophages form an immune suppressive niche via Treg induction and are associated with poor prognosis in breast cancer patients. **a** UMAP visualization of T cell subclusters colored by cell type. **b** Bar plot showing the relative abundance of each T cell subcluster in PyMT;control vs. PyMT;CXCR4$^{MΦ\text{-}cKO}$ groups. **c** Representative flow cytometry of FOXP3$^+$CD25$^+$ among CD4$^+$ cells (Regulatory T cell, Tregs) from preneoplastic glands. **d**, Quantification of FOXP3$^+$CD25$^+$CD4$^+$ Tregs by flow cytometry ($n = 3$, biologically independent samples). **e** CD45$^+$CD8$^+$ T cells in PyMT;control vs. PyMT;CXCR4$^{MΦ\text{-}cKO}$ glands ($n = 4$, 5, biologically independent samples). **f** Volcano plot of differentially expressed genes in CD8 T2 cluster from PyMT;control or PyMT;CXCR4$^{MΦ\text{-}cKO}$. Each dot represents a gene. Genes with absolute average $\log_2$ fold change > 0.5 and adjusted $p < 0.05$ are highlighted in colors. Representative upregulated genes in the cKO group are labeled. **g** The percentage of FOXP3$^+$CD25$^+$CD4$^+$ Tregs differentiated from naïve T cells in vitro by co-culturing of macrophages isolated from PyMT;-control and PyMT;CXCR4$^{MΦ\text{-}cKO}$ preneoplasia glands assessed by flow cytometry analysis ($n = 4$ in each group, biologically independent samples). **h** Percentage of FOXP3$^+$CD25$^+$CD4$^+$ Tregs differentiated from naïve T cells in vitro by co-culturing of CXCR4$^+$ and CXCR4- macrophages ($n = 4$, biologically independent samples). **i** Kaplan–Meier curve showing tumor onset in control ($n = 30$) and AMD3100 ($n = 30$) treated PyMT mice; two-tailed log-rank p-value and hazard ratio (HR). **j** Primary tumor growth in control ($n = 13$) and AMD3100-treated ($n = 17$) PyMT mice. **k** Quantification of lung metastases in the same groups as (**j**). **l** Kaplan–Meier survival analysis of breast cancer patients with all type or luminal B, HER2-positive, and basal subtype stratified by a 30-gene CXCR4$^+$MΦ signature derived from bulk RNA-seq of PyMT;control vs. PyMT;CXCR4$^{MΦ\text{-}cKO}$ preneoplasia glands. P value by two-tailed log-rank test and hazard ratio (HR) measured. Flow cytometry analysis of Tregs and CD8 T cells (Supplementary Fig. 16b) in (**c**–**e**, **g**, and **h**). Data are mean values ± s.d. Statistical significance calculated by two-tailed unpaired Student's t-test or one-way ANOVA with Turkey's test. Box plots show the median (center line), 25th/75th percentiles (box bounds), whiskers extending to 1.5× IQR, and outliers plotted individually. Source data are provided as a Source Data file.

brain metastasis[106]. Tissue-resident macrophages have emerged as a pivotal component of the MaSC niche, uniquely supporting the activity of MaSCs[23,35,36,39]. However, these studies employed global macrophage depletion approaches, such as CSF1 knockout or Clodronate liposomes treatment, and utilized markers, such as CSF1R, CCR2, and CX3CR1, which are broadly expressed in macrophages from other tissues and are not specifically enriched in mammary gland resident macrophages (Fig. 1a). Given the diversity and versatility of macrophages, there is an unmet need to identify a distinct macrophage subset that is specific for the MaSC niche and uniquely possesses MaSC-promoting functions, and to investigate their potential role in tumor initiation. Uncovering the specific signaling molecules that regulate the spatial arrangement and function of niche macrophages will help elucidate how TICs hijack MaSC-supporting functions of the niche to promote tumorigenesis. Furthermore, while adult stem cells and TICs are noted to enjoy an immune privileged status[30,31,87,89,107], how MaSC/TIC niche components support immune evasion of MaSC/TICs remains largely unknown.

In this study, we address these key questions by identifying CXCR4 as a phenotypic and functional marker of MaSC niche macrophages within the mammary ducts, with MaSC/TIC supporting functions. A unique tripartite CXCL12-CXCR4 chemokine signaling axis among macrophages, luminal, and basal cells within the mammary duct exists to recruit macrophages to the niche and prime them with MaSC-sustaining functions in normal mammary development, and further TIC-supporting functions during breast tumorigenesis (Supplementary Fig. 15). A specific subset of mammary gland macrophages express high levels of CXCR4 and are recruited to the mammary ducts through chemotaxis induced by luminal cell-derived CXCL12. CXCR4 signaling in macrophages activates AKT, which in turn phosphorylates β-catenin at Serine 552, leading to its stabilization and the activation of transcriptional activity. The downstream genes of β-catenin include pro-migratory genes such as MMP2, which facilitates invadopodia formation, ECM remodeling, and the insertion of CXCR4$^+$ macrophages into intraductal spaces. Activation of the β-catenin pathway in macrophages also induces the expression of pro-proliferation genes such as CCND3, and multiple Wnt ligands, including WNT2b, which signal basal/MaSCs to enhance their mammary stem cell properties (Supplementary Fig. 15). Importantly, we demonstrate the increased presence of the same CXCR4$^+$ niche macrophages in breast TIC niches and their critical roles during breast tumorigenesis. Similar to its role in the MaSC niche, CXCR4$^+$ niche macrophages promote TIC expansion and its tumor-initiating properties through the AKT–β-catenin–Wnt pathway. In addition, CXCR4 expression in niche macrophages induces immune-suppressive regulatory T cell differentiation and infiltration through elevated expression of ALDH1a2, mediating evasion of immune surveillance in early-stage tumors, and thus enabling tumor initiation and progression (Supplementary Fig. 15). The identification of CXCR4$^+$ macrophages as a specific stromal niche population for MaSCs and breast TICs represents a significant advance in our understanding of stromal niche for MaSC/TICs, parallel to the identification of unique niche components for other adult stem cell systems[57,101–104] or cancers[105,106].

CXCL12 and its cognate receptor CXCR4 play pivotal roles in the migration, polarization, proliferation, and survival of various cell types including hematopoietic cells and stem cells[54,55,108]. Furthermore, the CXCL12–CXCR4 axis and its downstream signaling pathways have been linked to tumorigenesis, metastasis, and interactions within the tumor microenvironment in various cancers, including breast cancer[55,109,110]. While a few studies have revealed the involvement of cytokine or chemokine signaling in mammary gland development[56,111,112] and tumorigenesis[75,113,114], a comprehensive investigation into the roles of CXCL12–CXCR4 chemokine signaling axis in forming the niche in support of mammary tissue renewal or tumor initiation remains absent to date. While CXCR4 expression in mammary cells[56] and tumors[75] has been previously reported, the regulation of the MaSC/TIC-supporting macrophageal niche through the significant impact of CXCL12–CXCR4 signaling on other non-macrophage cell types is unlikely. Through lineage-specific deletion of CXCR4 in macrophages and CXCL12 in luminal epithelial cells, we elucidated the critical role of macrophage CXCR4 in regulating both the spatial distribution of niche macrophages and the branching morphogenesis of mammary ducts, while having little effect on the CXCR4 expression in other cell types and their distribution. The deletion of CXCR4 in macrophages led to: (1) diminished epithelial association of macrophages, (2) compromised stem cell activity, primarily due to the loss of localized Notch-Wnt signaling, and (3) impaired branching morphogenesis and reduced terminal end buds. These findings align with the observed concentration of CXCR4-positive macrophages at the ductal branching points and the previously documented significant impact of stromal factors on branching events during development[115–117]. Given the multifaceted interactions macrophages can form with other niche cell types, it is possible that the deficient branching morphogenesis observed in CXCR4-cKO mice is partially attributable to reduced luminal cell proliferation or altered fibroblast-mediated ECM degradation, in addition to the impaired regenerative function of MaSC/basal cells. Direct reconstitution of CXCR4$^+$ macrophages into knockout mice could provide additional validation and help delineate the specific contributions of this macrophage subset to branching morphogenesis. These possibilities warrant further investigations.

In our pursuit to identify the cellular source of CXCL12 within the mammary epithelium, we encountered the unexpected discovery that luminal cells, instead of basal cells, express high levels of CXCL12. By acting as a source of CXCL12 to attract macrophages that support the stem cell activity of basal cells, luminal cells do not merely arise as progenies of MaSCs but actively contribute to the establishment of a

niche that sustains MaSCs. Notably, we observed marked similarities in both cellular phenotypes and gene expression profiles between $CXCR4^{M\Phi\text{-}cKO}$ and $CXCL12^{K8\text{-}cKO}$ mice, indicating that the survival and activation of $CXCR4^+$ macrophages are primarily regulated by CXCL12 secreted by luminal cells. However, given the heterogenous expression of CXCL12–CXCR4 across various cell types, it would be interesting to explore whether the expression levels and cellular localization of CXCR4–CXCL12 vary depending on different developmental stages, hormone milieus, and types of tumors. Furthermore, our gene expression analysis revealed upregulation of additional chemokine receptors, such as CXCR3 and CXCR6, in mammary gland macrophages compared to peritoneal macrophages (Fig. 1a), suggesting that other chemokine axes may contribute to stem cell niche maintenance. Further studies will be needed to systemically evaluate the broader chemokine network and potential compensatory mechanisms.

Wnt signaling is recognized as a fundamental pathway driving tissue renewal and stem cell activity across most adult tissues[38,118,119]. Several sources of niche Wnt have been identified during mammary gland development. Progesterone-induced Wnt4 in luminal cells and Wnt6 in basal cells likely play important roles in MaSC survival and function[69–72]. Our prior research pinpointed mammary macrophages as an important source of MaSC-promoting Wnt ligands, revealing that mammary gland macrophages enhance the production of Wnt ligands in response to Notch receptor activation by Dll1, which is prominently expressed in MaSCs[23]. Our current study indicates that these different sources of Wnt combine to optimally support MaSC activity. Given that stem cell-niche signaling, such as Notch and Wnt, often depends on juxtacrine or paracrine signaling between stem cells and stromal niche components, how such signaling events can occur is unclear if the mammary epithelium is physically isolated from stromal components by the basement membrane. Here, we revealed that activation of CXCR4–Akt signaling in macrophages not only stimulates their extracellular matrix (ECM) remodeling activity but also directly recruits them into the mammary epithelium via chemotaxis. AKT-mediated phosphorylation of β-catenin at Ser^{552} leads to the stabilization of β-catenin and the transcriptional activation of genes that promote macrophage proliferation, survival, migration, and Wnt production. The formation of MMP2-rich invadopodia facilitates macrophage transmigration across the basement membrane (BM), enabling direct cellular contact with luminal and basal cells/MaSCs. This process sustains a locally enriched Wnt-β-catenin signaling milieu that is instrumental in shaping the functions of both mammary epithelial cells and niche macrophages.

The function of tumor-associated macrophages (TAMs) in mammary tumorigenesis and progression has been extensively studied, mostly focusing on CSF1-CSF1R or CCL2-CCR2 signaling, which is broadly involved in the regulation of bone marrow-derived TAMs across various tissues[120–122] and are not particularly enriched in mammary resident macrophages (Fig. 1a). In this study, we highlight the tissue-specific role of $CXCR4^+$ macrophages in mammary glands and their direct impact on the survival and functional activity of breast tumor-initiating cells. We observed a progressive increase of $CXCR4^+$ macrophage during mammary tumorigenesis, possibly due to increased CXCL12 in other cell types such as fibroblasts during tumorigenesis. The functional importance of $CXCR4^+$ macrophage in breast cancer initiation was validated in multiple mouse models of breast cancer representing ER+, luminal B, and basal subtypes of breast cancer. Importantly, $CXCR4^+$ macrophages not only promote TIC activity but also create an immunosuppressive microenvironment by elevating the presence of Tregs. We also present molecular mechanisms demonstrating that $CXCR4^+$ macrophages upregulate ALDH1a2, which drives Treg differentiation and facilitates breast tumorigenesis. The identification of $CXCR4^+$ mammary gland niche macrophages that support breast TIC functions and the formation of an immune suppressive TIC niche is of great importance and could provide new insights for developing novel therapeutic or preventive treatments. Notably, our study highlights the potential therapeutic efficacy of targeting the CXCL12–CXCR4 axis using AMD 3100 or blocking ALDH1a2 with KyA33 in TIC-supporting macrophages to suppress mammary tumor onset and growth. Additionally, we confirm the correlation between the expression of $CXCR4^+$ macrophage signatures with poor survival of breast cancer patients, indicating that the level of infiltration of CXCR4-expressing macrophages could serve as a prognosis marker for breast cancer patients and a potential predictive marker for targeted therapy. Additional future validation of this prognosis analysis, including integrative genomic and scRNA-seq data to enable the inference of the abundance of $CXCR4^+$ macrophages based on bulk RNA transcriptomes, as well as immuno-histological analysis of patient samples to assess correlations with clinical outcomes, will facilitate the clinical development of such therapeutic strategy. Moreover, identifying additional downstream molecules responsible for $CXCR4^+$macrophage-mediating immune evasion, and targeting these pathways could improve current strategies to control cancer by targeting tumor-associated macrophages.

Methods

Ethical regulations

This study complies with all ethical regulations. All animal procedures presented in this study were approved by the Institutional Animal Care and Use Committee (IACUC, protocol 1881) at Princeton University and conducted in compliance with ethical standards and international guidelines for animal experimentation. In accordance with our approved IACUC protocol (1881), In vivo experiments were terminated at predefined time points or when mice reached human endpoints, including a single tumor reaching 20 mm in any dimension, a combined tumor volume of 4000 mm^3 in cases of multiple spontaneous tumors, >20% body weight loss, or signs of severe distress (lethargy, impaired mobility). Mice were monitored daily and euthanized according to IACUC-approved protocols when endpoint criteria were met.

Animal studies

All animals were housed and bred in an AALAC-approved SPF barrier facility using contemporary practices. Animal facility was maintained at 20–22 °C with 14 h:10 h light:dark cycles at 40–70% relative humidity. Mice were routinely tested for potentially confounding infections. Animal procedures were conducted in compliance with the Institutional Animal Care and Use Committee (IACUC, protocol 1881) of Princeton University. C57BL/6J, CXCR4-floxed, LysM-Cre, CXCL12-floxed, tamoxifen inducible-Krt8-Cre/ERT2, Krt14-Cre mice, MMTV-PyMT, and MMTV-WNT mice were obtained from Jackson Laboratory. For all animal experiments, 6–8-week-old females of wild-type, Cre control littermate, and knockout animals were utilized, unless otherwise indicated in the figure legend. Cre activity was induced in *Krt8*-Cre/ERT2 mice by a single injection of tamoxifen (1.5 mg) as reported previously[21]. Cre control littermates and $CXCL12^{K8\text{-}cKO}$ mice were given tamoxifen at 3–4 weeks of age and harvested after 3 or 10 weeks. For cleared fat-pad injection experiment, C57BL/6J wild-type mice at 3–4 weeks old were anaesthetized and a small incision was made to reveal the mammary gland. Mammary epithelial cells (MECs) as specified in each experiment were injected into cleared inguinal (#4) mammary fat pads according to the standard procedures[123,124]. For spontaneous tumorigenesis experiments, MMTV-PyMT or MMTV-WNT female mice with C57BL/6 J background were crossed with $CXCR4^{M\Phi\text{-}cKO}$ mice to generate knockout animals. PyMT;littermate controls and PyMT; $CXCR4^{M\Phi\text{-}cKO}$ mice were examined weekly for mammary tumors. For AMD3100 (Plerixafor) treatment, MMTV-PyMT mice were treated with either distilled water (control) or 0.06 mg/ml of AMD3100 in drinking water starting as early as 6 weeks of age for a

long-term treatment procedure. For in vivo KyA33 treatment, experimental mice were fed either a normal diet (control) or a diet supplemented with KyA33 (270 ppm, equivalent to an approximate dosing of 40 mg/kg in mice) until the completion of the experiment. Tumors were considered established when they became palpable for 2 consecutive weeks. For allograft studies, 8 weeks C57BL/6J females were used. Cells were suspended in 50% PBS and 50% Matrigel for mammary gland injection (MFP). Tumors were measured by calipers for the calculation of tumor volumes. Lung nodules were counted directly after fixation with Bouin's solution.

Cell lines

Py8119 and E0771 cells (C57BL/6J background) were obtained from the American Type Culture Collection (ATCC, Py8119: CRL-3278, E0771: CRL-3461). Py8119 was cultured in F-12K Medium containing 10% FBS, 20 ng/ml EGF, 5 µg/ml insulin, 2 µg/ml hydrocortisone, and 100 U penicillin/0.1 mg/ml streptomycin, while E0771 were cultured in RPMI-1640 medium with 10% FBS, 1% HEPES, and 100 U penicillin/ 0.1 mg/ml streptomycin.

Limiting dilution assay (LDA)

Primary cell suspension of mammary epithelial cells (MECs) isolated from 6 to 7-week-old wild-type (WT), Cre control littermates, $CXCR4^{M\phi\text{-}cKO}$ or $CXCL12^{K8\text{-}cKO}$ mammary glands were subjected to flow cytometry sorting using lineage makers (CD31, Ter119, and CD45), CD24, and CD29 to enrich for the MaSC-containing basal subsets ($Lin^-CD24^+CD29^{Hi}$). The sorted cells were then transplanted into cleared mammary fat pads of recipient Cre control littermates or $CXCR4^{M\phi\text{-}cKO}$ mice. Outgrowths were analyzed 6–8 weeks post-injection. Transplantation was performed with the indicated number of cells resuspended in a 1:1 mixture of Matrigel and PBS. The frequency of MaSCs in the injected cells was calculated using L-calc software (StemCell Technologies) or the ELDA (extreme limiting dilution assay)[19,125]. MaSC's self-renewal capacity was accessed by its ability to regenerate functional mammary glands in virgin mice following transplantation. For tumorigenesis assays, single-cell suspension of primary MECs from PyMT or WNT mice were transplanted into wild-type C57BL/6J, Cre control littermates, or $CXCR4^{M\phi\text{-}cKO}$ recipients. The same quantitative method was used in limiting dilution mammary fat pad injections to calculate TIC frequency in PyMT and WNT MECs.

Mammosphere assays/Tumorsphere assays

Single cells were plated in ultralow-attachment plates (Corning) with the standard mammosphere media[126]. The number of cells plated is indicated for each specific experiment in the figures. The spheres were counted 7–10 days later depending on the experiment. For co-culture mammosphere and tumorsphere assay, sorted MECs and macrophages were combined at a 1:4 ratio and cultured in mammosphere media on ultralow-attachment plates. This ratio was previously determined as the optimal in vitro coculture condition for macrophage-mediated enhancement of mammosphere formation by basal/MaSCs[23]. For the double- or triple-cell co-culture experiment, we utilized a transwell culture system. Tranwells with 0.4 µm pore inserts were placed in ultralow-attachment plates. Basal/MaSCs were seeded at the bottom, while macrophage and luminal cells were seeded on top of the insert, either separately or together, depending on the experimental setting.

Whole-mount staining of mammary glands

The 4th inguinal mammary glands were dissected, mounted on glass slides, and fixed overnight at room temperature in 10% formalin. After rehydration through a series of decreasing ethanol concentrations, tissues were stained overnight with Carmine Alum solution (0.2% carmine and 0.5% aluminum potassium sulfate). Stained-whole mounts were subsequently dehydrated in ethanol and cleared with a Histo-Clear solution. Images were acquired using a Zeiss microscope. Quantification of the lengths and numbers of branches was performed using ImageJ. The ductal length was measured as the distance between the lymph node and the distal end point of the longest duct. Ductal branching was quantified by manually counting the total number of branch nodes within 4–5 fields either adjacent to the sides of the lymph node for the mammary gland or randomly distributed for the reconstituted mammary gland. The manual counting was done in triplicate by three independent researchers including at least one blinded to the samples.

Immunohistochemistry (IHC), immunofluorescence (IF), and whole mount 3D IF

For histological analysis, mammary gland specimens were fixed overnight in neutral buffered formalin, dehydrated, and embedded in paraffin. Tissue blocks were sectioned into 5 µm. Antibodies and dilutions used for IHC and IF are listed in Supplementary Table 2. Sections from FFPE (formalin-fixed paraffin-embedded) specimens were dewaxed, rehydrated, and treated with target retrieval solution (Dako) according to the manufacturer's instructions. For IHC staining, after treatment with 3% H_2O_2 for 30 min to block endogenous peroxidase, slides were incubated with 3% bovine serum albumin for blocking, and incubated with primary antibodies at 4 °C overnight. Following washes with PBS, slides were then incubated with HRP-conjugated secondary antibody for 30 min at room temperature. Sections were stained by DAB and then counterstained with Hematoxylin. For IF staining, slides were blocked with 3% bovine serum albumin and incubated overnight with primary antibodies at 4 °C followed by Alexa Fluor-conjugated secondary antibody. The nuclei were counterstained with DAPI.

For whole-mount 3D IF staining[127], mammary glands from 8 to 9-week-old female mice were dissected and fixed in 4% paraformaldehyde (PFA) pH 7.4 for 2 h at 4 °C on a roller mixer. Tissues were washed in PBS with 0.1% Tween-20 for 10 min, then incubated for 30 min in wash buffer (WB) (PBS, 0.1% Tween-20, 50 mg/ml ascorbic acid, 0.05 ng/ml reduced L-Glutathione), followed by a 2–3 h incubation in WB1 (PBS, 0.2% Tween, 0.2% Triton, 0.02% SDS, 0.2% BSA, 50 mg/ml ascorbic acid, 0.05 ng/ml reduced L-glutathione) at 4 °C. Primary antibodies were diluted 1:50 in cold WB2 (PBS, 0.1% Triton, 0.02% SDS, 0.2% BSA, 50 mg/ml ascorbic acid, 0.05 ng/ml L-Glutathione) and incubated overnight at 4 °C in vertically positioned tubes on an orbital mixer. The next day, tissues were washed three times in WB2 at 4 °C, with fresh buffer changes every hour. Secondary antibodies were diluted 1:100–1:200 in cold WB2 and incubated overnight under the same conditions. After three additional washes, samples were incubated in FUnGI clearing solution (50% glycerol (vol/vol), 2.5 M fructose, 2.5 M urea, 10.6 mM Tris Base, 1 mM EDTA, supplemented with 50 mg/ml ascorbic acid, 0.05 ng/ml L-glutathione) in 15 ml conical tubes placed horizontally on an orbital mixer overnight at 4 °C in the dark. Tissues were then mounted between a coverslip and slide for analysis. Images were taken using a Nikon A1 confocal microscope and a Zeiss fluorescence microscope. Representative images from more than ten images per specimen were selected.

Flow cytometry and FACS sorting

Single mammary epithelial cells (MECs) and macrophages were obtained from mammary glands after excising the lymph node, following the published protocol[23,28]. MECs were stained with a combination of lineage (CD45, Ter119, and CD31), CD24, and CD29 antibodies, macrophages were stained with CD45, CD11b, F4/80 or/and CXCR4, Tregs were stained with CD45, CD4, CD25 and FOXP3 for 20–30 min. The gating strategy is shown in Supplementary Fig. 16. For intracellular staining, single cells were fixed with either BD Fix/Perm or eBioscience Foxp3/Transcription factor staining buffer set according

to the kit instructions. For sorting cells, the FACSAria Fusion (BD Biosciences) instrument was used. Flow cytometry analysis was performed using the LSRII or FACSymphony A3 (BD Biosciences). All data were acquired using FACSDiva software and were analyzed using FlowJo software. Detection of CXCL12 mRNA and protein in MECs was performed with PrimeFlow™ RNA Assay Kit (Thermo Fisher Scientific) in accordance with the manufacturer's instructions. Details about all FACS-related antibodies are listed in Supplementary Table 2.

Transwell cell migration assay

Cell migration was accessed using a Boyden-chamber transwell system with 8 μm pore polycarbonate membrane inserts (Corning). FACS-sorted macrophages were seeded in the upper chamber in 200 μl RPMI containing 2% FBS and 1% penicillin–streptomycin. The lower chamber contained either culture media or FACS-sorted luminal cells in RPMI with 10% FBS and 1% penicillin–streptomycin. After 24 h incubation, migrated cells on the bottom of the membrane were fixed, stained with 1% crystal violet, and washed three times with distilled water. Images were captured using a Zeiss microscope, and migration was quantified using ImageJ software.

Invadopodia assay

QGM gelatin invadopodia assay kit (EMD Millipore) was used by following the manufacturer's instructions. Briefly, eight-well glass chamber slides were coated with a thin layer of fluorescent-conjugated gelatins according to the manufacturer's protocol. Seeded cells were fixed in 4% paraformaldehyde (PFA) and stained with DAPI and Phalloidin. The quantification of gelatin degradation areas was performed with Image J Thresholding.

In vitro Treg differentiation assay

$CD4^+$ T cells were isolated from wild-type spleens using Miltenyi Biotec Naive $CD4^+$ T cell Isolation Kit following the manufacturer's instructions. 100,000 naïve $CD4^+$ T cells were co-cultured with 50,000 sorted primary macrophages and the percentage of differentiated Tregs was examined by flow cytometry analysis 5–7 days later.

Aldefluor assay

Aldefluor assay was carried out following the manufacturer's instructions with some adjustments (STEMCELL Technologies #01700). Briefly, FACS-sorted macrophages for testing were resuspended in Aldefluor assay buffer with DEAB (Sigma) (100 μM), DMSO (1%), or ALDH inhibitor, KyA33 (1 μM) and incubated in 37 °C for 40 min. Cells were then centrifuged and resuspended in 1 μg/ml DAPI containing aldefluor assay buffer and subjected to flow cytometry analysis. DEAB group was used to determine the background fluorescence signal and set the accurate gating for $ALDH^+$ cells.

RNA purification and qRT-PCR analyses

Total RNA was extracted from primary cells using the Qiagen RNA extraction kit, following the manufacturer's protocol. Quantitative real-time PCR was performed using SYBR Green Supermix (Bio-Rad) on ABI 7900 96 HT series and StepOne Plus systems (Applied Biosystem). The gene-specific primer sets are listed in Supplementary Table 3 and were used at a final concentration of 0.2 mM. All qRT-PCR assays were performed in triplicate in at least two independent experiments.

RNA sequencing and GSEA analysis

Total RNA from FACS-isolated cells directly sorted into lysis reagent was purified using the RNAeasy micro kit (Qiagen) according to the manufacturer's instructions. The integrity of total RNA samples was assessed on Bioanalyzer 2100 using an RNA 6000 Pico chip (Agilent Technologies, CA). Messenger RNA was enriched from these samples using QIAseq FastSelect-rRNA HMR Kit (Qiagen, CA), fragmented, and converted to cDNA and Illumina sequencing library using the PrepX RNA-seq library preparation protocol on the Apollo 324TM NGS Library Prep System (Takara Bio, CA). A unique DNA barcode was incorporated into each library for sample demultiplexing. These RNA-seq libraries were examined on Agilent Bioanalyzer DNA High Sensitivity chips for size distribution, quantified by Qubit fluorometer (Invitrogen, CA), and pooled at equal molar amounts. The library pools were denatured and sequenced on Illumina NovaSeq 6000 using the S Prime flowcells as pair-end 65 nt reads according to the manufacturer's protocol. Raw sequencing reads were filtered by Illumina NovaSeq Control Software, only the Pass-Filter (PF) reads were de-multiplexed allowing 1 mismatch, and used for further analysis. Alignment of reads was done using the STAR aligner with the mm10 build of the mouse genome. Transcript assembly and differential expression were determined using DESeq2 with Refseq mRNAs to guide assembly. Data was deconvoluted and analyzed with the Partek Flow software (Partek Inc.) and the GeneSpring 13 software (Agilent). For GSEA and pathway analysis, normalized Log2 ratio expression data was first rank-ordered by differential expression. Only datasets with nominal $P < 0.05$ were considered in the analysis. Data was analyzed using GSEA_v4.1.0. Interrogated signatures from the MySigDB v6.0 C2 curated gene sets database. "The mammary gland macrophage signature" from Chakrabarti et al. (2018) and "MaSC signature and luminal cell signature" from Chakrabarti et al. (2014) are derived from the microarray data collected from our lab as described in previous study[23,28].

Single-cell RNA sequencing

Single-cell suspensions were accessed for cell density and viability using a FACSymphony A3 (BD Biosciences) or Attune (Thermo Fisher Scientific) flow cytometer. Approximately 15,000 cells per sample were loaded into each channel of the 10X Genomics Chromium X system using the Chromium Single Cell 3' v3.1 Reagent Kits (10X Genomics) for cDNA generation and amplification. Amplified cDNA was purified with Ampure XP magnetic beads (Beckman Coulter), quantified using a Qubit fluorometer (Invitrogen), and accessed for size distribution with a Bioanalyzer with High Sensitivity DNA chips (Agilent). Illumina sequencing libraries were prepared using the Tagment DNA Enzyme and Buffer kit (Illumina), quantified by Qubit and Bioanalyzer, pooled at equal-molar concentrations, and sequenced on an Illumina NovaSeq 6000 S Prime flow cell (28 + 94 nt pair-end reads) following standard protocols. Pass-filter reads were obtained using Illumina NovaSeq Control Software, and subsequent demultiplexing and gene expression quantification were performed using CellRanger software (10X Genomics) to generate gene expression and quality control matrices.

Analysis of single-cell RNA sequencing dataset

Data preprocessing, normalization, integration, and clustering of single-cell RNA-seq data were performed using the Seurat package (version 5.0.0)[128]. In our initial preprocessing, all samples were filtered by selecting cells with more than 200 but fewer than 5000 detected genes. Additionally, the genes not expressed in at least 3 cells were excluded. As a quality control, cells expressing more than 15% mitochondrial genes were filtered out. Furthermore, a Scrublet[129] cutoff of 0.25 was used to account for and filter doublets in each sample. Sample normalization and integration were done using the 2000 most variable genes per sample. Following sample integration, unsupervised clustering was done based on the shared-nearest neighbor method. Louvain clustering with a resolution of 0.8, which initially identified 25 distinct clusters. Similar cell subtypes were manually merged to identify 10 major cell type clusters. The cell types are visualized using UMAP-based dimensional reduction. To identify marker genes within each cluster, the FindAllMarkers function from Seurat was used with a logFC cutoff value of 0.25. Canonical markers were used to identify main cell types, followed by sub-clustering to identify cell subtypes. For differential gene expression analysis, a single-cell aggregation

approach with edgeR[130] was done, and a fold-change of at least 1.5 and an adjusted *p*-value of <0.05 cutoffs were used to select differentially expressed genes across different conditions. All plots were done using either standard Seurat plotting functions or the ggplot2 package within the core tidiverse in R (1.3.0).

Analysis of published single-cell or bulk RNA sequencing dataset

We downloaded the dataset of Li, C.M. et al. (2020) (GSE150580), Kumar, T. et al. (2023) (GSE195665), and Dawon, C.A. et al. (2020) (GSE119869). Single-cell analysis was done with Seurat (v4.4.0) and R (v4.2.2). Bulk RNA-seq analysis was done with DESeq2 (v1.38.0). Normalized counts were calculated by DESeq2 during DEG (differentially expressed genes) analysis.

Statistics and reproducibility

All statistical comparisons were conducted with GraphPad Prism version 10 (Student *t*-test, Mann–Whitney *U,* and two-way ANOVA) and Microsoft Excel. Results are represented as indicated in the figure legends, generally as mean ± SD (standard deviation). For experiments with two groups, a small sample size (<30), and normally distributed data, the significance was evaluated using a two-tailed unpaired Student's *t*-test under the assumption of unequal variance. All statistical comparisons are non-significant at an alpha level of 0.05 if not marked by a specific *p*-value or asterisk. For multiple independent groups, one-way ANOVA with Turkey's multiple comparisons test was evaluated. Non-parametric data sets were evaluated using the Mann–Whitney Wilcoxon *U* test. For in vitro experiments, no statistical method was used to predetermine sample size; all samples were analyzed equally, and randomization was not required. Repopulation frequency was calculated using ELDA software with Pearson's chi-squared test (two-sided). For survival analysis, long-rank (*P*) tests were applied. All experiments with representative images (FACS plot, immunofluorescence, and histology) were repeated independently at least three times and representative images were shown. Tissue staining scores were assessed by three independent, blinded researchers. For animal studies, no statistical test was used to predetermine sample size; group sizes were informed by pilot and prior studies. Littermates were randomized before injection, using animals of similar age and female sex. Researchers were not blinded to group allocation or outcomes, as knowledge of treatment groups was necessary for the procedures. Animals were excluded only if they died or had to be euthanized because of moribund conditions following the IACUC protocol.

Reporting summary

Further information on research design is available in the Nature Portfolio Reporting Summary linked to this article.

Data availability

The RNA sequencing data generated in this study have been deposited in the NCBI Gene Expression Omnibus (GEO) database under the accession code GSE275908, and accessed at https://www.ncbi.nlm.nih.gov/geo/query/acc.cgi?acc=GSE275908. Source data are provided with this paper.

References

1. Liu, X., Li, W., Fu, X. & Xu, Y. The immunogenicity and immune tolerance of pluripotent stem cell derivatives. *Front. Immunol.* **8**, 645 (2017).
2. Magee, J. A., Piskounova, E. & Morrison, S. J. Cancer stem cells: impact, heterogeneity, and uncertainty. *Cancer Cell* **21**, 283–296 (2012).
3. Clarke, M. F. et al. Cancer stem cells-perspectives on current status and future directions: AACR Workshop on cancer stem cells. *Cancer Res.* **66**, 9339–9344 (2006).
4. Kreso, A. & Dick, J. E. Evolution of the cancer stem cell model. *Cell Stem Cell* **14**, 275–291 (2014).
5. Nguyen, L. V., Vanner, R., Dirks, P. & Eaves, C. J. Cancer stem cells: an evolving concept. *Nat. Rev. Cancer* **12**, 133–143 (2012).
6. Visvader, J. E. & Stingl, J. Mammary stem cells and the differentiation hierarchy: current status and perspectives. *Genes Dev.* **28**, 1143–1158 (2014).
7. Inman, J. L., Robertson, C., Mott, J. D. & Bissell, M. J. Mammary gland development: cell fate specification, stem cells and the microenvironment. *Development* **142**, 1028–1042 (2015).
8. Shackleton, M. et al. Generation of a functional mammary gland from a single stem cell. *Nature* **439**, 84–88 (2006).
9. Stingl, J. et al. Purification and unique properties of mammary epithelial stem cells. *Nature* **439**, 993–997 (2006).
10. Sreekumar, A., Roarty, K. & Rosen, J. M. The mammary stem cell hierarchy: a looking glass into heterogeneous breast cancer landscapes. *Endocr. Relat. Cancer* **22**, T161–176 (2015).
11. Fu, N. Y., Nolan, E., Lindeman, G. J. & Visvader, J. E. Stem Cells and the Differentiation Hierarchy in Mammary Gland Development. *Physiol. Rev.* **100**, 489–523 (2020).
12. Van Keymeulen, A. et al. Distinct stem cells contribute to mammary gland development and maintenance. *Nature* **479**, 189–193 (2011).
13. van Amerongen, R., Bowman, A. N. & Nusse, R. Developmental stage and time dictate the fate of Wnt/beta-catenin-responsive stem cells in the mammary gland. *Cell Stem Cell* **11**, 387–400 (2012).
14. Wuidart, A. et al. Early lineage segregation of multipotent embryonic mammary gland progenitors. *Nat. Cell Biol.* **20**, 666–676 (2018).
15. Spike, B. T. et al. A mammary stem cell population identified and characterized in late embryogenesis reveals similarities to human breast cancer. *Cell Stem Cell* **10**, 183–197 (2012).
16. Scheele, C. L. et al. Identity and dynamics of mammary stem cells during branching morphogenesis. *Nature* **542**, 313–317 (2017).
17. Van Keymeulen, A. et al. Lineage-restricted mammary stem cells sustain the development, homeostasis, and regeneration of the estrogen receptor positive lineage. *Cell Rep.* **20**, 1525–1532 (2017).
18. Wang, C., Christin, J. R., Oktay, M. H. & Guo, W. Lineage-biased stem cells maintain estrogen-receptor-positive and -negative mouse mammary luminal lineages. *Cell Rep.* **18**, 2825–2835 (2017).
19. Asselin-Labat, M. L. et al. Control of mammary stem cell function by steroid hormone signalling. *Nature* **465**, 798–802 (2010).
20. Plaks, V. et al. Lgr5-expressing cells are sufficient and necessary for postnatal mammary gland organogenesis. *Cell Rep.* **3**, 70–78 (2013).
21. Rios, A. C., Fu, N. Y., Lindeman, G. J. & Visvader, J. E. In situ identification of bipotent stem cells in the mammary gland. *Nature* **506**, 322–327 (2014).
22. Wang, D. et al. Identification of multipotent mammary stem cells by protein C receptor expression. *Nature* **517**, 81–84 (2015).
23. Chakrabarti, R. et al. Notch ligand Dll1 mediates cross-talk between mammary stem cells and the macrophageal niche. *Science* **360,** eaan4153 (2018).
24. Liu, C. et al. Niche inflammatory signals control oscillating mammary regeneration and protect stem cells from cytotoxic stress. *Cell Stem Cell* **31**, 89–105.e106 (2024).
25. Guo, W. et al. Slug and Sox9 cooperatively determine the mammary stem cell state. *Cell* **148**, 1015–1028 (2012).
26. Chakrabarti, R. et al. Elf5 inhibits the epithelial–mesenchymal transition in mammary gland development and breast cancer metastasis by transcriptionally repressing Snail2. *Nat. Cell Biol.* **14**, 1212–1222 (2012).

27. Singh, S. et al. Loss of ELF5-FBXW7 stabilizes IFNGR1 to promote the growth and metastasis of triple-negative breast cancer through interferon-gamma signalling. *Nat. Cell Biol.* **22**, 591–602 (2020).
28. Chakrabarti, R. et al. DeltaNp63 promotes stem cell activity in mammary gland development and basal-like breast cancer by enhancing Fzd7 expression and Wnt signalling. *Nat. Cell Biol.* **16**, 1004–1015 (2014). 1001-1013.
29. Kumar, S. et al. DeltaNp63-driven recruitment of myeloid-derived suppressor cells promotes metastasis in triple-negative breast cancer. *J. Clin. Investig.* **128**, 5095–5109 (2018).
30. Celia-Terrassa, T. et al. Normal and cancerous mammary stem cells evade interferon-induced constraint through the miR-199a-LCOR axis. *Nat. Cell Biol.* **19**, 711–723 (2017).
31. Perez-Nunez, I. et al. LCOR mediates interferon-independent tumor immunogenicity and responsiveness to immune-checkpoint blockade in triple-negative breast cancer. *Nat. Cancer* **3**, 355–370 (2022).
32. Wang, D. et al. Protein C receptor is a therapeutic stem cell target in a distinct group of breast cancers. *Cell Res.* **29**, 832–845 (2019).
33. Kumar, S. et al. Dll1(+) quiescent tumor stem cells drive chemoresistance in breast cancer through NF-kappaB survival pathway. *Nat. Commun.* **12**, 432 (2021).
34. Kumar, S. et al. Estrogen-dependent DLL1-mediated Notch signaling promotes luminal breast cancer. *Oncogene* **38**, 2092–2107 (2019).
35. Gyorki, D. E., Asselin-Labat, M. L., van Rooijen, N., Lindeman, G. J. & Visvader, J. E. Resident macrophages influence stem cell activity in the mammary gland. *Breast Cancer Res.* **11**, R62 (2009).
36. Gouon-Evans, V., Rothenberg, M. E. & Pollard, J. W. Postnatal mammary gland development requires macrophages and eosinophils. *Development* **127**, 2269–2282 (2000).
37. Fuchs, E. & Blau, H. M. Tissue stem cells: architects of their niches. *Cell Stem Cell* **27**, 532–556 (2020).
38. Clevers, H., Loh, K. M. & Nusse, R. Stem cell signaling. An integral program for tissue renewal and regeneration: Wnt signaling and stem cell control. *Science* **346**, 1248012 (2014).
39. Dawson, C. A. et al. Tissue-resident ductal macrophages survey the mammary epithelium and facilitate tissue remodelling. *Nat. Cell Biol.* **22**, 546–558 (2020).
40. Lu, P., Takai, K., Weaver, V. M. & Werb, Z. Extracellular matrix degradation and remodeling in development and disease. *Cold Spring Harb. Perspect. Biol.* **3**, a005058 (2011).
41. Walma, D. A. C. & Yamada, K. M. The extracellular matrix in development. *Development* **147**, dev175596 (2020).
42. Bleriot, C., Chakarov, S. & Ginhoux, F. Determinants of resident tissue macrophage identity and function. *Immunity* **52**, 957–970 (2020).
43. Nalio Ramos, R. et al. Tissue-resident FOLR2(+) macrophages associate with CD8(+) T cell infiltration in human breast cancer. *Cell* **185**, 1189–1207.e1125 (2022).
44. Vogel, A. & Weichhart, T. Tissue-resident macrophages - early passengers or drivers in the tumor niche?. *Curr. Opin. Biotechnol.* **83**, 102984 (2023).
45. Zhu, Y. et al. Tissue-resident macrophages in pancreatic ductal adenocarcinoma originate from embryonic hematopoiesis and promote tumor progression. *Immunity* **47**, 323–338.e326 (2017).
46. Casanova-Acebes, M. et al. Tissue-resident macrophages provide a pro-tumorigenic niche to early NSCLC cells. *Nature* **595**, 578–584 (2021).
47. Kumar, T. et al. A spatially resolved single-cell genomic atlas of the adult human breast. *Nature* **620**, 181–191 (2023).
48. Li, C. M. et al. Aging-associated alterations in mammary epithelia and stroma revealed by single-cell RNA sequencing. *Cell Rep.* **33**, 108566 (2020).
49. Clausen, B. E., Burkhardt, C., Reith, W., Renkawitz, R. & Forster, I. Conditional gene targeting in macrophages and granulocytes using LysMcre mice. *Transgenic Res.* **8**, 265–277 (1999).
50. Nie, Y. et al. The role of CXCR4 in maintaining peripheral B cell compartments and humoral immunity. *J. Exp. Med.* **200**, 1145–1156 (2004).
51. McWhorter, F. Y., Davis, C. T. & Liu, W. F. Physical and mechanical regulation of macrophage phenotype and function. *Cell. Mol. Life Sci.* **72**, 1303–1316 (2015).
52. McWhorter, F. Y., Wang, T., Nguyen, P., Chung, T. & Liu, W. F. Modulation of macrophage phenotype by cell shape. *Proc. Natl Acad. Sci. USA* **110**, 17253–17258 (2013).
53. Cai, S. et al. A quiescent Bcl11b high stem cell population is required for maintenance of the mammary gland. *Cell Stem Cell* **20**, 247–260.e245 (2017).
54. Bianchi, M. E. & Mezzapelle, R. The chemokine receptor CXCR4 in cell proliferation and tissue regeneration. *Front. Immunol.* **11**, 2109 (2020).
55. Shi, Y., Riese, D. J. 2nd & Shen, J. The role of the CXCL12/CXCR4/CXCR7 chemokine axis in cancer. *Front. Pharm.* **11**, 574667 (2020).
56. Shiah, Y. J. et al. A progesterone–CXCR4 axis controls mammary progenitor cell fate in the adult gland. *Stem Cell Rep.* **4**, 313–322 (2015).
57. Greenbaum, A. et al. CXCL12 in early mesenchymal progenitors is required for haematopoietic stem-cell maintenance. *Nature* **495**, 227–230 (2013).
58. Wang, J. & Knaut, H. Chemokine signaling in development and disease. *Development* **141**, 4199–4205 (2014).
59. Britton, C., Poznansky, M. C. & Reeves, P. Polyfunctionality of the CXCR4/CXCL12 axis in health and disease: Implications for therapeutic interventions in cancer and immune-mediated diseases. *FASEB J.* **35**, e21260 (2021).
60. Janssens, R., Struyf, S. & Proost, P. The unique structural and functional features of CXCL12. *Cell. Mol. Immunol.* **15**, 299–311 (2018).
61. Malsin, E. S., Kim, S., Lam, A. P. & Gottardi, C. J. Macrophages as a source and recipient of Wnt signals. *Front. Immunol.* **10**, 1813 (2019).
62. Feng, Y. et al. Wnt/beta-catenin-promoted macrophage alternative activation contributes to kidney fibrosis. *J. Am. Soc. Nephrol.* **29**, 182–193 (2018).
63. Fang, D. et al. Phosphorylation of beta-catenin by AKT promotes beta-catenin transcriptional activity. *J. Biol. Chem.* **282**, 11221–11229 (2007).
64. Zheng, H. et al. TREM2 promotes microglial survival by activating Wnt/beta-Catenin pathway. *J. Neurosci.* **37**, 1772–1784 (2017).
65. He, X. C. et al. PTEN-deficient intestinal stem cells initiate intestinal polyposis. *Nat. Genet.* **39**, 189–198 (2007).
66. Wang, Y. et al. Tissue-resident macrophages promote extracellular matrix homeostasis in the mammary gland stroma of nulliparous mice. *Elife* **9**, e57438 (2020).
67. Stewart, T. A., Hughes, K., Hume, D. A. & Davis, F. M. Developmental stage-specific distribution of macrophages in mouse mammary gland. *Front. Cell Dev. Biol.* **7**, 250 (2019).
68. Linder, S., Cervero, P., Eddy, R. & Condeelis, J. Mechanisms and roles of podosomes and invadopodia. *Nat. Rev. Mol. Cell Biol.* **24**, 86–106 (2023).
69. Brisken, C. et al. Essential function of Wnt-4 in mammary gland development downstream of progesterone signaling. *Genes Dev.* **14**, 650–654 (2000).
70. Joshi, P. A. et al. Progesterone induces adult mammary stem cell expansion. *Nature* **465**, 803–807 (2010).
71. Rajaram, R. D. et al. Progesterone and Wnt4 control mammary stem cells via myoepithelial crosstalk. *EMBO J.* **34**, 641–652 (2015).

72. Roarty, K., Pfefferle, A. D., Creighton, C. J., Perou, C. M. & Rosen, J. M. Ror2-mediated alternative Wnt signaling regulates cell fate and adhesion during mammary tumor progression. *Oncogene* **36**, 5958–5968 (2017).
73. Plaks, V., Kong, N. & Werb, Z. The cancer stem cell niche: how essential is the niche in regulating stemness of tumor cells?. *Cell Stem Cell* **16**, 225–238 (2015).
74. Prager, B. C., Xie, Q., Bao, S. & Rich, J. N. Cancer stem cells: the architects of the tumor ecosystem. *Cell Stem Cell* **24**, 41–53 (2019).
75. Zhang, M. et al. Intratumoral heterogeneity in a Trp53-null mouse model of human breast cancer. *Cancer Discov.* **5**, 520–533 (2015).
76. Ortiz, M. M. O. & Andrechek, E. R. Molecular characterization and landscape of breast cancer models from a multi-omics perspective. *J. Mammary Gland Biol. Neoplasia* **28**, 12 (2023).
77. Orimo, A. et al. Stromal fibroblasts present in invasive human breast carcinomas promote tumor growth and angiogenesis through elevated SDF-1/CXCL12 secretion. *Cell* **121**, 335–348 (2005).
78. Davie, S. A. et al. Effects of FVB/NJ and C57Bl/6J strain backgrounds on mammary tumor phenotype in inducible nitric oxide synthase deficient mice. *Transgenic Res.* **16**, 193–201 (2007).
79. Regua, A. T., Arrigo, A., Doheny, D., Wong, G. L. & Lo, H. W. Transgenic mouse models of breast cancer. *Cancer Lett.* **516**, 73–83 (2021).
80. Asselin-Labat, M. L. et al. Gata-3 is an essential regulator of mammary-gland morphogenesis and luminal-cell differentiation. *Nat. Cell Biol.* **9**, 201–209 (2007).
81. Lim, E. et al. Transcriptome analyses of mouse and human mammary cell subpopulations reveal multiple conserved genes and pathways. *Breast Cancer Res.* **12**, R21 (2010).
82. Yeo, S. K. et al. Single-cell RNA-sequencing reveals distinct patterns of cell state heterogeneity in mouse models of breast cancer. *Elife* **9**, e58810 (2020).
83. Wan, L. et al. MTDH–SND1 interaction is crucial for expansion and activity of tumor-initiating cells in diverse oncogene- and carcinogen-induced mammary tumors. *Cancer Cell* **26**, 92–105 (2014).
84. Herschkowitz, J. I. et al. Identification of conserved gene expression features between murine mammary carcinoma models and human breast tumors. *Genome Biol.* **8**, R76 (2007).
85. Le Naour, A. et al. EO771, the first luminal B mammary cancer cell line from C57BL/6 mice. *Cancer Cell Int.* **20**, 328 (2020).
86. Gibby, K. et al. Early vascular deficits are correlated with delayed mammary tumorigenesis in the MMTV-PyMT transgenic mouse following genetic ablation of the NG2 proteoglycan. *Breast Cancer Res.* **14**, R67 (2012).
87. Agudo, J. & Miao, Y. Stemness in solid malignancies: coping with immune attack. *Nat. Rev. Cancer* **25**, 27–40 (2024).
88. Goto, N. et al. SOX17 enables immune evasion of early colorectal adenomas and cancers. *Nature* **627**, 636–645 (2024).
89. Miao, Y. et al. Adaptive immune resistance emerges from tumor-initiating stem cells. *Cell* **177**, 1172–1186.e1114 (2019).
90. Barker, N. et al. Crypt stem cells as the cells-of-origin of intestinal cancer. *Nature* **457**, 608–611 (2009).
91. Flesken-Nikitin, A. et al. Ovarian surface epithelium at the junction area contains a cancer-prone stem cell niche. *Nature* **495**, 241–245 (2013).
92. Martincorena, I. et al. Tumor evolution. High burden and pervasive positive selection of somatic mutations in normal human skin. *Science* **348**, 880–886 (2015).
93. Fujisaki, J. et al. In vivo imaging of Treg cells providing immune privilege to the haematopoietic stem-cell niche. *Nature* **474**, 216–219 (2011).
94. Cohen, J. N. et al. Regulatory T cells in skin mediate immune privilege of the hair follicle stem cell niche. *Sci. Immunol.* **9**, eadh0152 (2024).
95. Gil Del Alcazar, C. R. et al. Immune escape in breast cancer during in situ to invasive carcinoma transition. *Cancer Discov.* **7**, 1098–1115 (2017).
96. Lal, A. et al. FOXP3-positive regulatory T lymphocytes and epithelial FOXP3 expression in synchronous normal, ductal carcinoma in situ, and invasive cancer of the breast. *Breast Cancer Res. Treat.* **139**, 381–390 (2013).
97. Lavin, Y. et al. Innate immune landscape in early lung adenocarcinoma by paired single-cell analyses. *Cell* **169**, 750–765.e717 (2017).
98. Soroosh, P. et al. Lung-resident tissue macrophages generate Foxp3+ regulatory T cells and promote airway tolerance. *J. Exp. Med.* **210**, 775–788 (2013).
99. Zhu, B. et al. IL-4 and retinoic acid synergistically induce regulatory dendritic cells expressing Aldh1a2. *J. Immunol.* **191**, 3139–3151 (2013).
100. Gyorffy, B. et al. An online survival analysis tool to rapidly assess the effect of 22,277 genes on breast cancer prognosis using microarray data of 1,809 patients. *Breast Cancer Res. Treat.* **123**, 725–731 (2010).
101. Ding, L. & Morrison, S. J. Haematopoietic stem cells and early lymphoid progenitors occupy distinct bone marrow niches. *Nature* **495**, 231–235 (2013).
102. Ding, L., Saunders, T. L., Enikolopov, G. & Morrison, S. J. Endothelial and perivascular cells maintain haematopoietic stem cells. *Nature* **481**, 457–462 (2012).
103. Goto, N. et al. Lymphatics and fibroblasts support intestinal stem cells in homeostasis and injury. *Cell Stem Cell* **29**, 1246–1261.e1246 (2022).
104. McCarthy, N. et al. Distinct mesenchymal cell populations generate the essential intestinal BMP signaling gradient. *Cell Stem Cell* **26**, 391–402.e395 (2020).
105. Su, S. et al. CD10(+)GPR77(+) cancer-associated fibroblasts promote cancer formation and chemoresistance by sustaining cancer stemness. *Cell* **172**, 841–856.e816 (2018).
106. Priego, N. et al. STAT3 labels a subpopulation of reactive astrocytes required for brain metastasis. *Nat. Med.* **24**, 1024–1035 (2018).
107. Baldominos, P. et al. Quiescent cancer cells resist T cell attack by forming an immunosuppressive niche. *Cell* **185**, 1694–1708.e1619 (2022).
108. Sugiyama, T., Kohara, H., Noda, M. & Nagasawa, T. Maintenance of the hematopoietic stem cell pool by CXCL12-CXCR4 chemokine signaling in bone marrow stromal cell niches. *Immunity* **25**, 977–988 (2006).
109. Hughes, R. et al. Perivascular M2 macrophages stimulate tumor relapse after chemotherapy. *Cancer Res* **75**, 3479–3491 (2015).
110. Arwert, E. N. et al. A Unidirectional transition from migratory to perivascular macrophage is required for tumor cell intravasation. *Cell Rep.* **23**, 1239–1248 (2018).
111. Wilson, G. J. et al. Atypical chemokine receptor ACKR2 controls branching morphogenesis in the developing mammary gland. *Development* **144**, 74–82 (2017).
112. Wilson, G. J. et al. Chemokine receptors coordinately regulate macrophage dynamics and mammary gland development. *Development* **147**, dev187815 (2020).
113. Chia, K., Mazzolini, J., Mione, M. & Sieger, D. Tumor initiating cells induce Cxcr4-mediated infiltration of pro-tumoral macrophages into the brain. *Elife* **7**, e31918 (2018).
114. Taniguchi, S. et al. Tumor-initiating cells establish an IL-33-TGF-beta niche signaling loop to promote cancer progression. *Science* **369**, eaay1813 (2020).

115. Goodwin, K. & Nelson, C. M. Branching morphogenesis. *Development* **147**, dev184499 (2020).
116. Wiseman, B. S. & Werb, Z. Stromal effects on mammary gland development and breast cancer. *Science* **296**, 1046–1049 (2002).
117. Zhao, C. et al. Stromal Gli2 activity coordinates a niche signaling program for mammary epithelial stem cells. *Science* **356**, eaal3485 (2017).
118. Reya, T. & Clevers, H. Wnt signalling in stem cells and cancer. *Nature* **434**, 843–850 (2005).
119. Turashvili, G., Bouchal, J., Burkadze, G. & Kolar, Z. Wnt signaling pathway in mammary gland development and carcinogenesis. *Pathobiology* **73**, 213–223 (2006).
120. Qian, B. Z. et al. CCL2 recruits inflammatory monocytes to facilitate breast-tumour metastasis. *Nature* **475**, 222–225 (2011).
121. Kitamura, T. et al. CCL2-induced chemokine cascade promotes breast cancer metastasis by enhancing retention of metastasis-associated macrophages. *J. Exp. Med.* **212**, 1043–1059 (2015).
122. Lewis, C. E., Harney, A. S. & Pollard, J. W. The multifaceted role of perivascular macrophages in tumors. *Cancer Cell* **30**, 18–25 (2016).
123. Deome, K. B., Faulkin, L. J. Jr., Bern, H. A. & Blair, P. B. Development of mammary tumors from hyperplastic alveolar nodules transplanted into gland-free mammary fat pads of female C3H mice. *Cancer Res.* **19**, 515–520 (1959).
124. Chakrabarti, R. & Kang, Y. Transplantable mouse tumor models of breast cancer metastasis. *Methods Mol. Biol.* **1267**, 367–380 (2015).
125. Lim, E. et al. Aberrant luminal progenitors as the candidate target population for basal tumor development in BRCA1 mutation carriers. *Nat. Med.* **15**, 907–913 (2009).
126. Dontu, G. et al. In vitro propagation and transcriptional profiling of human mammary stem/progenitor cells. *Genes Dev.* **17**, 1253–1270 (2003).
127. Rios, A. C. et al. Intraclonal plasticity in mammary tumors revealed through large-scale single-cell resolution 3D imaging. *Cancer Cell* **35**, 618–632.e616 (2019).
128. Hao, Y. et al. Dictionary learning for integrative, multimodal and scalable single-cell analysis. *Nat. Biotechnol.* **42**, 293–304 (2024).
129. Zeisel, A. et al. Brain structure. Cell types in the mouse cortex and hippocampus revealed by single-cell RNA-seq. *Science* **347**, 1138–1142 (2015).
130. Chen, Y., Lun, A. T. & Smyth, G. K. From reads to genes to pathways: differential expression analysis of RNA-Seq experiments using Rsubread and the edgeR quasi-likelihood pipeline. *F1000Research* **5**, 1438 (2016).

Acknowledgements

We thank J.A. Volmar, J.M. Miller, and W. Wang at The Lewis-Sigler Institute Genomics Core Facility for RNA sequencing, S. Wang and G. Laevsky at the Confocal Imaging Facility of Princeton University for assistance with imaging, and C. DeCoste at the Flow Cytometry Resource Facility of Princeton University for flow cytometry analysis. We thank Kelly Walton, Lucyann Franciosa, and Shafiq Bhat at The Biospecimen Repository and Histopathology resource of the Rutgers Cancer Institute of New Jersey for histological analysis support. This work was supported by postdoctoral fellowships from the NJCCR (COCR23PDF015) to E. Lee and the Brewster Foundation, and grants from Ludwig Cancer Research, the Breast Cancer Research Foundation, the NIH (R01CA134519), Department of Defense Breast Cancer Research Program (BC151403), American Cancer Society, and Susan G. Komen Foundation to Y. Kang. This research was also supported by the Flow Cytometry Resource Facility of Princeton University (NIH 1S10OD028592-01A1).

Author contributions

E.L. conceived the project and co-wrote the manuscript. E.L. and J.J.H. designed and performed the experiments, and analyzed data, with assistance from Y.W. G.S.V., N.S., and C.L.T. analyzed the single-cell and bulk RNA sequencing data. X.H. performed tissue processing and sectioning. J.A.V., J.M.M., and W.W. conducted RNA sequencing. S.W. and G.L. assisted with confocal imaging and analysis. C.J.D. assisted with flow cytometry and FACS experiments. Y.K. conceived and supervised the project, designed the experiments, and co-wrote the manuscript.

Competing interests

Y.K. is a co-founder and chair of the Scientific Advisory Board of Firebrand Therapeutics, Inc. and Kayothera, Inc. The remaining authors declare no competing interests.

Additional information

Supplementary information The online version contains supplementary material available at https://doi.org/10.1038/s41467-025-59972-z.

Correspondence and requests for materials should be addressed to Yibin Kang.

Peer review information *Nature Communications* thanks Jeffrey Rosen, and the other, anonymous, reviewer(s) for their contribution to the peer review of this work. A peer review file is available.